

Drastic facilitation of the onset of global chaos between separatrices of a Hamiltonian system

S.M. Soskin,^{1,2,*} R. Mannella,³ and O.M. Yevtushenko²

¹*Institute of Semiconductor Physics, National Academy of Sciences of Ukraine, 03028 Kiev, Ukraine*

²*Abdus Salam ICTP, 34100 Trieste, Italy*

³*Dipartimento di Fisica, Università di Pisa, 56127 Pisa, Italy*

We present the *self-consistent* theory describing the earlier discovered (PRL 90, 174101 (2003)) drastic facilitation of the onset of global chaos in time periodically perturbed Hamiltonian systems possessing two separatrices. The minimal perturbation amplitude that provides for chaotic transport between the separatrices possesses deep spikes as a function of the perturbation frequency. The relevant mechanism is the following: each of the two chaotic layers associated with the separatrices overlaps in the phase space one of the two relevant nonlinear resonances whilst the resonances reconnect with each other. We develop the self-contained theory for the boundaries of chaotic layers in the asymptotic limit of small distance in energy between the separatrices. On the base of this theory, we *explicitly* describe the spikes in the vicinity of the minima. We also discuss a few applications: the increase of the dc conductivity of the 2D electron gas in a magnetic superlattice, the acceleration of the noise-induced spatial diffusion of cold atoms in an optical lattice, the facilitation of the stochastic web formation in a wave-driven or kicked oscillator.

PACS numbers: 05.45.-a, 05.45.Ac, 05.45.Pq

I. INTRODUCTION

A weak perturbation of a Hamiltonian system causes the onset of chaotic layers around separatrices of the unperturbed system and/or separatrices surrounding nonlinear resonances generated by the perturbation itself [1, 2, 3]. The system may be transported along the layer random-like and such a chaotic transport plays an important role in many physical phenomena [3]. If the perturbation is sufficiently weak, then the layers are thin and such chaos is called *local* [1, 2, 3]. As the magnitude of the perturbation increases, the width of the layer grows and the layers corresponding to adjacent separatrices (either to those of the unperturbed system or to separatrices surrounding different nonlinear resonances) reconnect at some, typically non-small, critical value of the magnitude. This conventionally marks the onset of *global* chaos [1, 2, 3] i.e. chaos in a large region of the phase space and an intensive chaotic transport through the whole relevant energy range. The reconnection of the layers around separatrices of the unperturbed system is schematically shown in Fig. 1. The reconnection of the layers around separatrices of the resonances often correlates with the overlap in energy between neighbouring resonances calculated independently in the resonant approximations of the corresponding orders (Fig. 2). The latter constitutes the Chirikov resonance-overlap criterion [1, 2, 3].

The Chirikov criterion may fail in time-periodically perturbed *zero-dispersion* (ZD) systems [4] (cf. also studies of related maps [5, 6]) i.e. systems in which the frequency of eigenoscillation possesses a local maximum or minimum as a function of its energy. In such systems, there are typically two resonances of one and the same order [7], and their overlap in energy does not result in the onset of global chaos [4, 5, 6]. Even their overlap in phase space [8] results typically only in reconnection of the thin chaotic layers associated with the resonances. As the amplitude of the time-periodic perturbation grows further, the layers may *separate* again [4, 5, 6]. An example of the evolution of resonances in the plane of energy and slow angle is given in Fig. 3 (the typical evolution of a real Poincaré section is shown e.g. in [9]).

It was recently suggested in our letter [10] that, in order for the global chaos to occur in a zero-dispersion system, the energy range relevant to the overlap of resonances of the same order should be *confined* between chaotic layers relating either to resonances of a different order [11] or to separatrices of the unperturbed system. These scenarios immediately suggest the corresponding substitute for the Chirikov criterion in a ZD system in the range of the local maximum/minimum. The onset of global chaos occurs respectively in a broader energy range or at *unusually small* magnitudes of the perturbation. Whilst the former case will be considered elsewhere, the present work develops the detailed self-consistent theory of the latter case as well as discusses generalizations and applications. Preliminary results were presented in a brief form in proceedings [12].

*Also at Physics Department, Lancaster University, UK

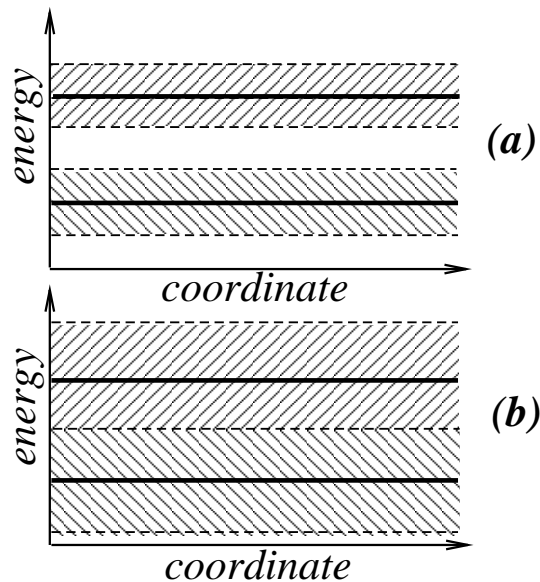


FIG. 1: Schematically shown conventional scenario of the onset of global chaos between separatrices of the unperturbed system as the perturbation magnitude grows. The width of chaotic layers (shaded) around the separatrices (solid lines) grows until the layers reconnect.

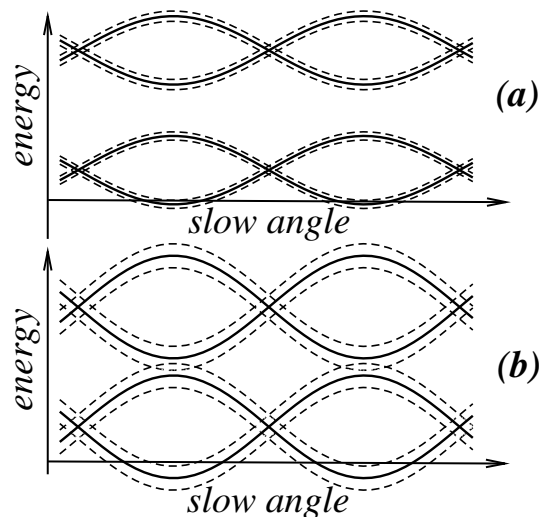


FIG. 2: Schematically shown conventional scenario of the onset of global chaos in accordance with the Chirikov criterion. Separatrices of resonances are schematically drawn by thick solid lines while the chaotic layers surrounding them are indicated by shaded areas.

The paper is organized as follows. Sec. II introduces the model and presents the major results of simulations. We study numerically the frequency dependence of the minimal amplitude of the ac drive at which the global chaos occurs, $h_{gc}(\omega_f)$. The simulations demonstrate that $h_{gc}(\omega_f)$ possesses deep spikes at certain frequencies. Sec. III gives the self-consistent asymptotic theory for the very minima of the spikes. Sec. IV gives the theory for the wings of the spikes. Discussion of a few generalizations and possible applications is carried in Sec. V. Conclusions are drawn in Sec. VI. The Appendix presents the analysis of the separatrix map in the relevant range of the perturbation parameters.

II. MODEL AND MAJOR RESULTS OF SIMULATIONS

Major results of our work are relevant to any one-dimensional Hamiltonian system possessing two or more separatrices and being subjected to a time-periodic perturbation [13]. As an example of an unperturbed system, we use a

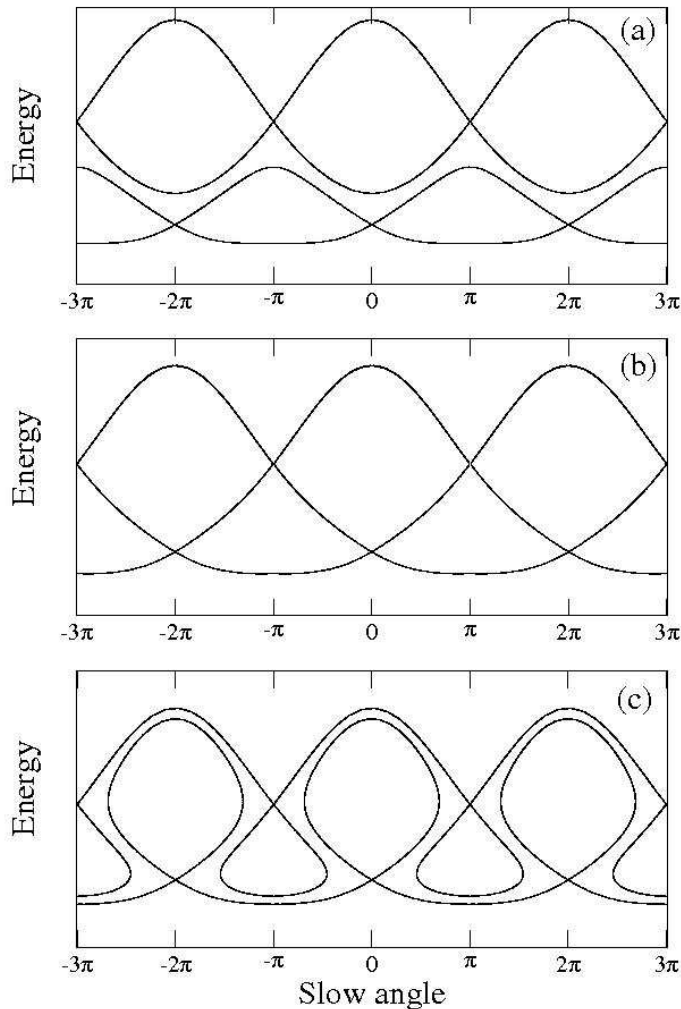


FIG. 3: Typical evolution of thin chaotic layers in the plane of slow variables of a zero-dispersion system (the perturbation magnitude grows from the top to the bottom).

spatially periodic potential system with two different-height barriers per period (Fig. 4(a)):

$$H_0(p, q) = \frac{p^2}{2} + U(q), \quad U(q) = \frac{(\Phi - \sin(q))^2}{2},$$

$$\Phi = \text{const} < 1. \quad (1)$$

This model may relate e.g. to a classical 2D electron gas in a magnetic field spatially periodic in one of the in-plane dimensions [14]. The interest to this system arose yet in the 90th due to technological advances allowing to manufacture high-quality magnetic superlattices [15, 16] leading to a variety of interesting behaviours of charge carriers in semiconductors (see [14, 15, 16, 17, 18] and references therein). The dynamics of a pendulum spinning about its vertical axis reduces to the model (1) too [19].

Figs. 4(b) and 4(c) show respectively the separatrices of the Hamiltonian system (1) in the $p - q$ plane and the dependence of the frequency ω of its oscillation, often called *eigenfrequency*, on energy $E \equiv H_0(p, q)$. The separatrices correspond to the energies equal to the potential barriers levels $E_b^{(1)} \equiv (1 - \Phi)^2/2$ and $E_b^{(2)} \equiv (1 + \Phi)^2/2$ (Fig. 4(a)). The function $\omega(E)$ is close to the extreme eigenfrequency $\omega_m \equiv \omega(E_m)$ in the major part of the interval $[E_b^{(1)}, E_b^{(2)}]$ while sharply decreasing to zero as E approaches $E_b^{(1)}$ or $E_b^{(2)}$.

Let the time-periodic perturbation be added. As an example, we use the ac drive, that corresponds to the perturbation of the dipole type [3, 20]:

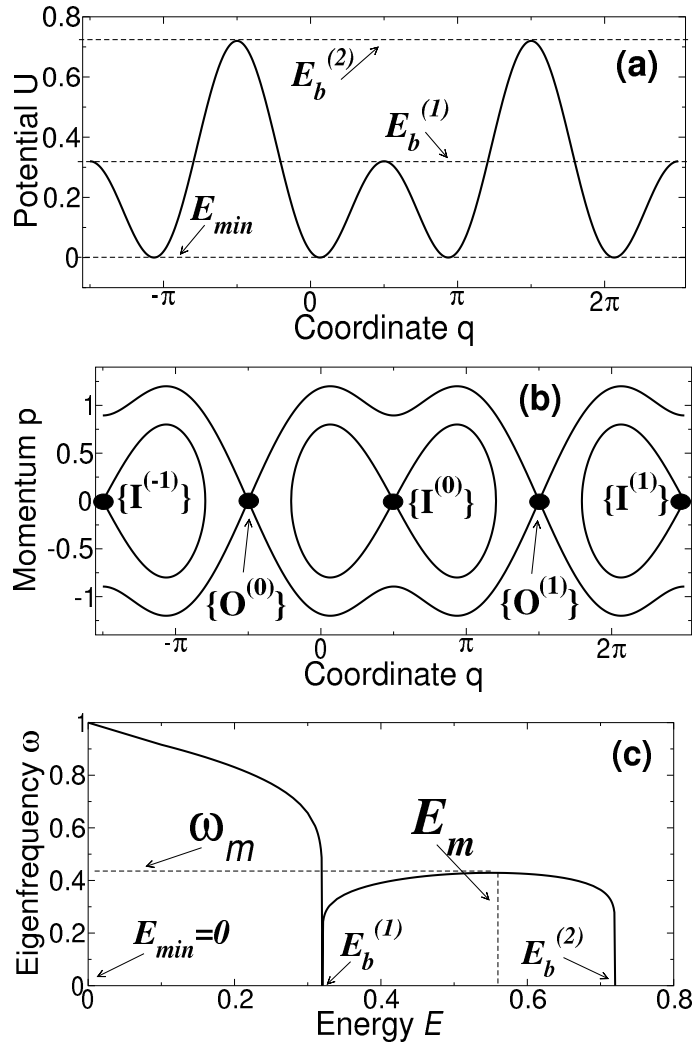


FIG. 4: The potential $U(q)$, the separatrices in the phase space and the eigenfrequency $\omega(E)$ for the unperturbed system (1) with $\Phi = 0.2$, in (a), (b) and (c) respectively.

$$\begin{aligned} \dot{q} &= \partial H / \partial p, & \dot{p} &= -\partial H / \partial q, \\ H(p, q) &= H_0(p, q) - hq \cos(\omega_f t). \end{aligned} \quad (2)$$

The *conventional* scenario of the onset of global chaos in the system (2)-(1) is illustrated by Fig. 5. The figure presents the evolution of the stroboscopic Poincaré section as h grows while ω_f is fixed at an arbitrarily chosen value *beyond* the vicinity of ω_m and its harmonics. At small h , there are two thin chaotic layers around the inner and outer separatrices of the unperturbed system. The layers are *homogeneous* on a coarse-grain scale. Unbounded chaotic transport takes place only in the outer chaotic layer i.e. in a *narrow* energy range. As h grows, so do also the layers, still remaining homogeneous on the coarse-grain scale. At some critical value $h_{gc} \equiv h_{gc}(\omega_f)$, they merge. This may be considered as the onset of global chaos: the whole range of energies between the barriers levels is involved in unbounded chaotic transport. The states $\{I^{(l)}\} \equiv \{p = 0, q = \pi/2 + 2\pi l\}$ and $\{O^{(l)}\} \equiv \{p = 0, q = -\pi/2 + 2\pi l\}$ (where l is any integer) in the Poincaré section are associated respectively with the inner and outer saddles of the unperturbed system, and necessarily belong to the inner and outer chaotic layers respectively. Thus, the necessary and sufficient condition for the global chaos to arise may be formulated as the possibility for the system placed initially in the state $\{I^{(0)}\}$ to pass beyond the neighbouring “outer” states, $\{O^{(0)}\}$ or $\{O^{(1)}\}$, i.e. for the coordinate q to become $< -\pi/2$ or $> 3\pi/2$ at sufficiently large times $t \gg 2\pi/\omega_f$.

A diagram in the $h - \omega_f$ plane, based on the above criterion, is shown in Fig. 6. The lower boundary of the shaded

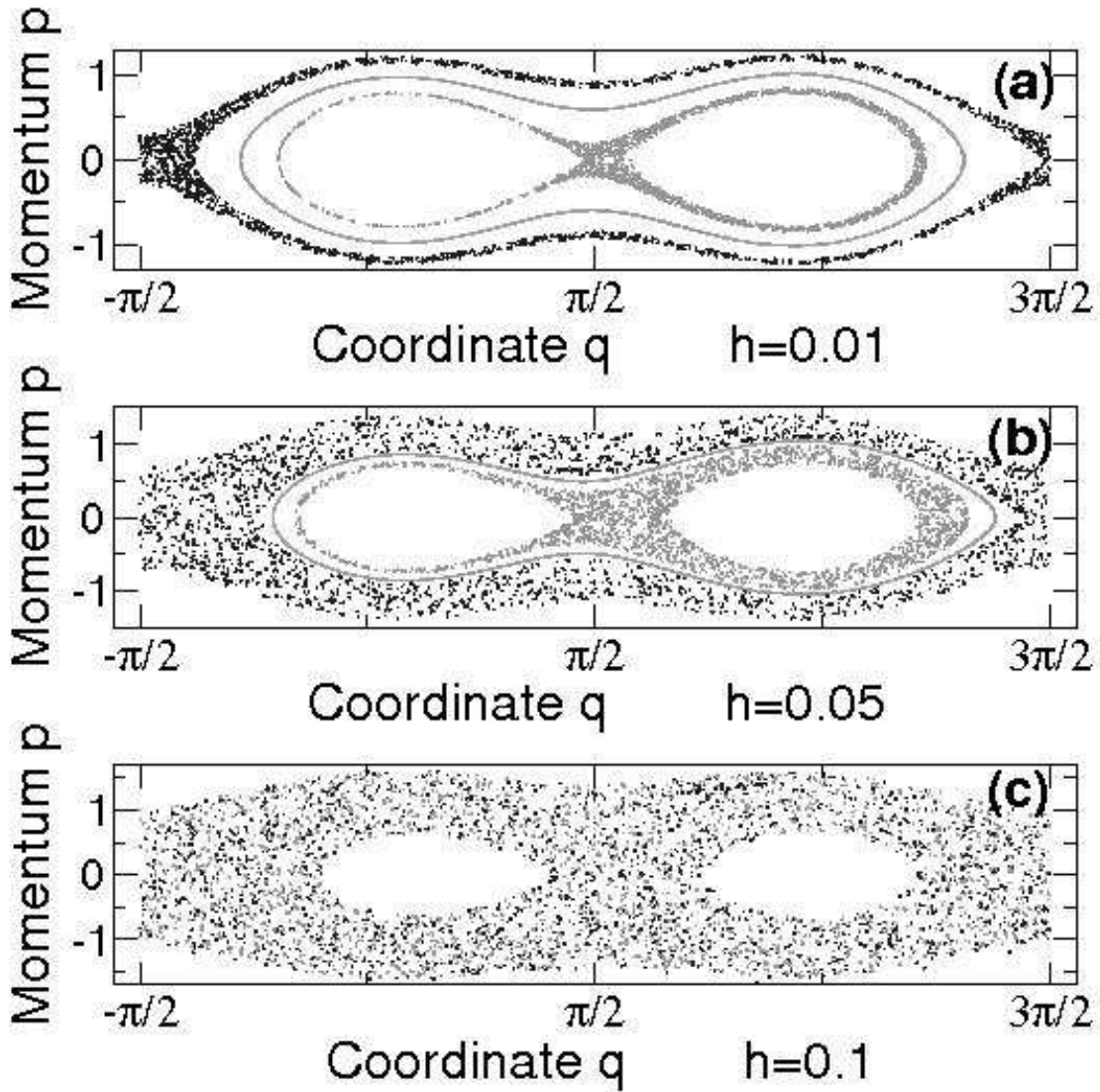


FIG. 5: The evolution of the stroboscopic (for $t = n2\pi/\omega_f$ with $n = 0, 1, 2, \dots$) Poincaré sections of the system (2)-(1) at $\Phi = 0.2$, with $\omega_f = 0.3$, as h grows from the top to the bottom: (a) 0.01, (b) 0.05, (c) 0.1. The number of points in each trajectory is 2000. In parts (a) and (b), three characteristic trajectories are shown: the inner trajectory starts from the state $\{I^{(0)}\} \equiv \{p = 0, q = \pi/2\}$ and is chaotic but bounded in the space; the outer trajectory starts from $\{O^{(0)}\} \equiv \{p = 0, q = -\pi/2\}$ and is chaotic and unbounded in coordinate; the third trajectory is an example of a regular trajectory separating the above chaotic ones. In (c), the chaotic trajectories mix.

area represents the function $h_{gc}(\omega_f)$. It has deep cusp-like local minima (*spikes*) the major of which are situated at frequencies $\omega_f = \omega_s^{(j)}$ that are slightly less than the odd multiples of ω_m ,

$$\omega_s^{(j)} \approx \omega_m(2j - 1), \quad j = 1, 2, \dots \quad (3)$$

The deepest minimum occurs at $\omega_s^{(1)} \approx \omega_m$: the value of h_{gc} in the minimum, $h_s^{(1)} \equiv h_{gc}(\omega_s^{(1)})$, is approximately 40 times smaller than the value in the neighbouring pronounced local maximum of $h_{gc}(\omega_f)$ at $\omega_f \approx 1$. As n increases, an n th minimum becomes less deep. The function $h_{gc}(\omega_f)$ is very sensitive to ω_f in the vicinity of the minima: for example, a shift of ω_f down from $\omega_s^{(1)} \approx 0.4$ by only 1% causes the increase of h_{gc} by $\approx 30\%$.

The origin of the spikes becomes more clear if to follow the evolution of the Poincaré section at $\omega_f \approx \omega_s^{(1)}$ as h grows: it drastically differs from the conventional evolution shown in Fig. 5. An example of such an evolution is shown

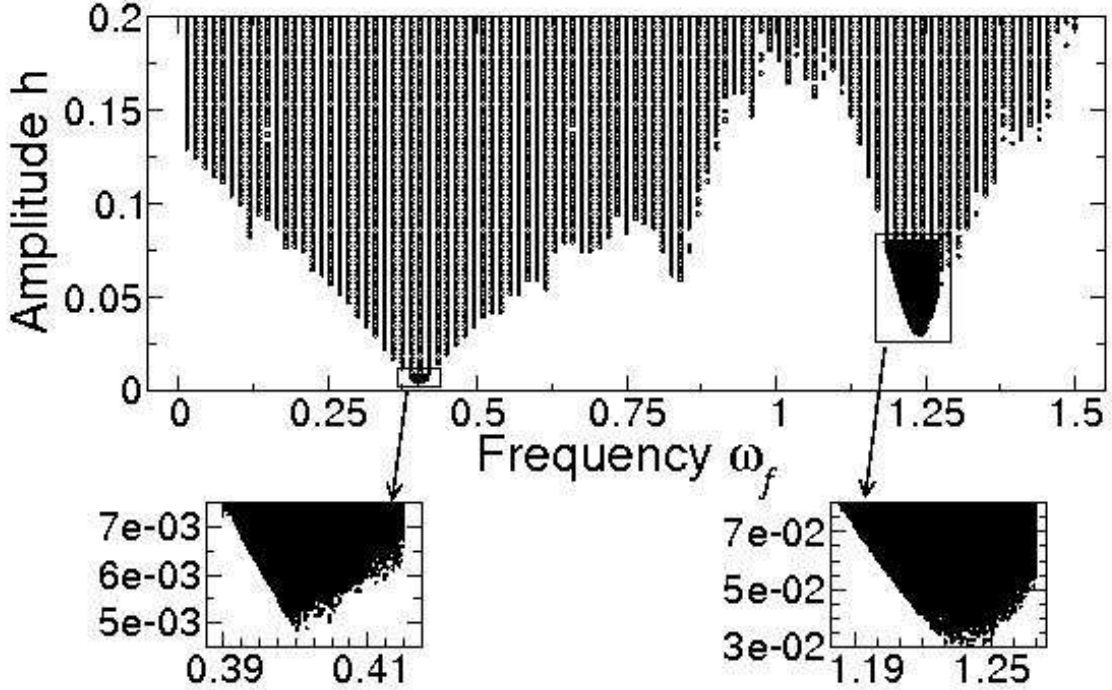


FIG. 6: The diagram indicating (by shading) the perturbation parameters ranges at which global chaos exists. Integration time for each point of the grid is 12000π .

in Fig. 7. For $h = 0.001$, Fig. 7(a), one can see four chaotic trajectories. Two of them, as conventionally (cf. Fig. 5), are associated with the inner and outer separatrices of the unperturbed system. They are marked by green and blue respectively. These trajectories fill the corresponding chaotic layers, which will be referred below as the “inner” and “outer” separatrix layers respectively. The other two chaotic trajectories marked by red and cyan are associated with the two nonlinear resonances of the 1st order. Examples of non-chaotic trajectories separating the chaotic ones are shown in brown. As the perturbation amplitude h increases, the outer separatrix layer sequentially absorbs other chaotic trajectories while large stability islands (associated with the resonances) arise in the layer. At $h = 0.003$, it has absorbed the red trajectory: the resulting chaotic layer is shown in blue in Fig. 7(b). At $h = 0.00475$, the latter layer has absorbed the cyan chaotic trajectory: the resulting chaotic layer is shown in blue in Fig. 7(c) [21]. Finally, at $h = 0.0055$ the latter blue layer has merged with the inner separatrix layer [22] (see Fig. 7(d)), i.e. the onset of global chaos as defined above has occurred.

Even prior the theoretical analysis, one can draw a few important conclusions from the evolution. Namely, if the frequency is close to the minimum of the spike of $h_{gc}(\omega_f)$,

- (1) the onset of global chaos occurs due to the *combination* of the overlap of chaotic layers associated with nonlinear resonances with each other and the overlap of the latter layers with the inner and outer separatrix layers.
- (2) the width of the nonlinear resonances becomes large already at quite *small* amplitudes of the perturbation, so that the overlap with chaotic layers around the original separatrices occurs at unusually small perturbation amplitudes;
- (3) the onset of the overlap of at least one of the nonlinear resonances with the outer separatrix layer occurs at values of h which are a few times smaller than those required for the onset of the overlap with the inner separatrix layer; hence, in order to find the minimal h at which the nonlinear resonances overlap *both* layers, it is sufficient to seek just the overlap with the *inner* separatrix layer: the outer separatrix layer would necessarily be overlapped at such h too.

The above conclusions are also illustrated by Fig. 8 which presents the evolution of the phase space of slow variables [1, 2, 3, 4], action $I \equiv I(E)$ and slow angle $\psi \equiv \psi - \omega_f t$, calculated in the resonance approximation of the 1st order (see Eq. (4) below).

Similarly, for the spikes of the higher order, higher-order resonances are relevant.

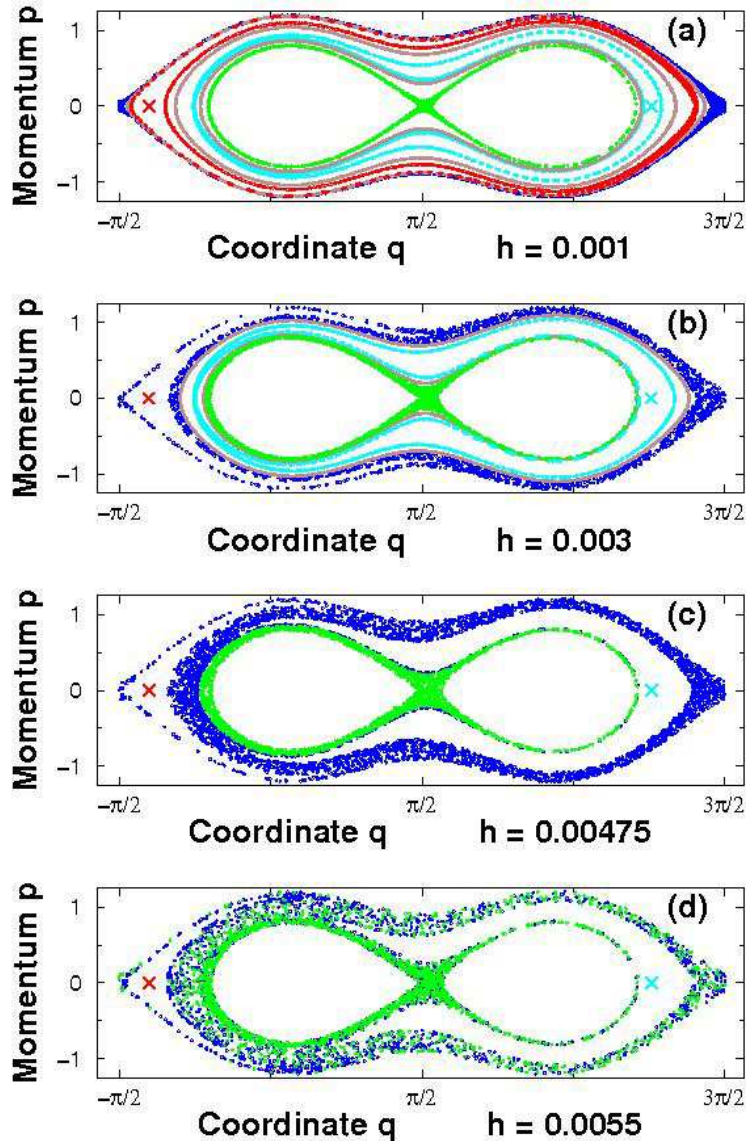


FIG. 7: The evolution of the stroboscopic Poincaré section of the system (2)-(1) with $\Phi = 0.2$ as the amplitude of the perturbation h grows while the frequency is fixed at $\omega_f = 0.401$. The number of points in each trajectory is 2000. The chaotic trajectories starting from the states $\{I^{(0)}\}$ and $\{O^{(0)}\}$ are drawn in green and blue respectively. The stable stationary points of Eq. (14) (the 1st-order nonlinear resonances) are indicated by the red and cyan crosses. The chaotic layers associated with the resonances are indicated in red and cyan respectively, unless they do not merge with those associated with the green/blue chaotic trajectories. Examples of regular trajectories embracing the state $\{I^{(0)}\}$ while separating various chaotic trajectories are shown in brown.

Two next sections are devoted to the theory describing spikes of the function $h_{gc}(\omega_f)$. Given that the most interesting and important parts of the spikes are their minima, we devote to the minima the whole Sec. III, deriving the explicit asymptotic expressions. In Sec. IV, we present the theory of the “wings” of the spikes.

III. EXPLICIT ASYMPTOTIC THEORY FOR THE MINIMA OF THE SPIKES

The eigenfrequency $\omega(E)$ is close to its local maximum ω_m in the most of the relevant range $[E_b^{(1)}, E_b^{(2)}]$ (Fig.4(c)). As shown below, $\omega(E)$ approaches a *rectangular* form in the asymptotic limit $\Phi \rightarrow 0$. Hence, if the perturbation

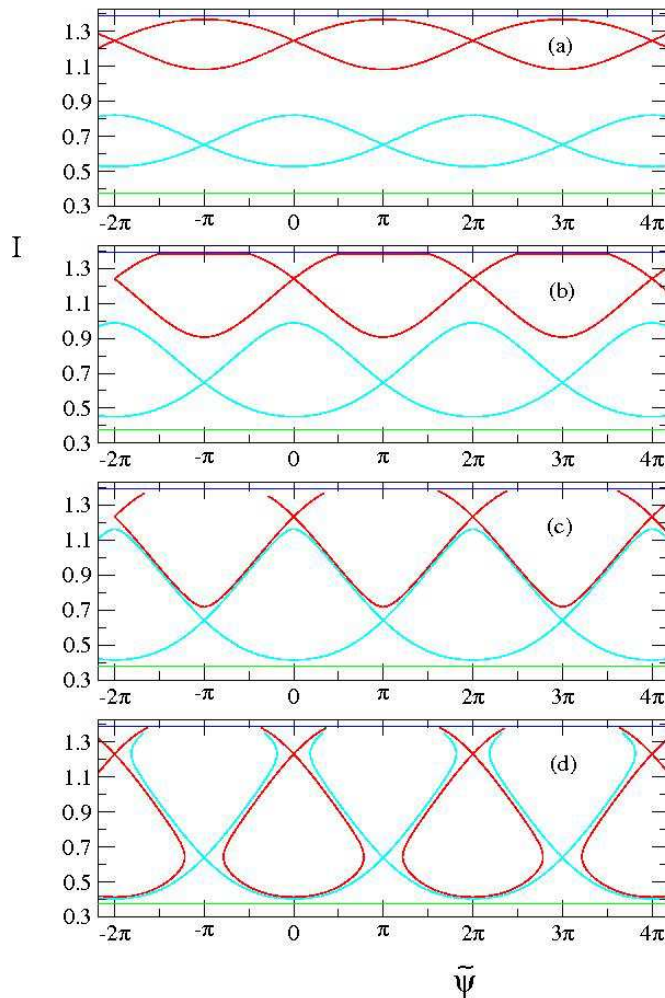


FIG. 8: The evolution of the separatrices (full lines) of the 1st-order resonances within the resonance approximation (described by the Hamiltonian (4) with $n = 1$) in the plane of action I and slow angle $\tilde{\psi}$, for the same parameters as in Fig. 7. The horizontal lines show the barriers levels.

frequency ω_f is close to ω_m or its odd multiples, $|\omega_f - \omega_m(2j - 1)| \ll \omega_m$, the energy width of nonlinear resonances becomes comparable with the width of the whole relevant range between barriers (i.e. $E_b^{(2)} - E_b^{(1)} \approx 2\Phi$) at a rather small perturbation magnitude $h \ll \Phi$. Note that the parameter Φ determines a characteristic order of the perturbation magnitude required for the conventional overlap of the separatrix chaotic layers, when ω_f is not close to any odd multiple of ω_m (Fig. 5 (c)).

Thus, the nonlinear resonances should play a crucial role in the onset of global chaos if $\omega_f \approx \omega_s^{(j)}$ (cf. Fig. 7). Moreover, chaotic layers associated with separatrices of nonlinear resonances are very narrow [1, 2, 3] (much narrower than those associated with the separatrices of the unperturbed system); and therefore it is sufficient to approximate their evolution merely by the evolution of the separatrices of nonlinear resonances.

On the other hand, as it has been demonstrated in the previous section, it is essential for the separatrices of nonlinear resonances to nearly touch the barriers energy levels, while the resonance approximation is obviously invalid in the very close vicinity of the barriers. Therefore, it is not obvious *a priori* whether it is indeed possible to describe $h_{gc}(\omega_f \approx \omega_s^{(j)})$ within the resonance approximation. Besides, numerical calculations of resonances show that, if $\omega_f \approx \omega_s^{(j)}$, the perturbation amplitude h required for the resonance separatrix to touch a given energy level in the close vicinity of the barrier level is very sensitive to ω_f . This may seem to make the task to calculate $h_s^{(j)} \equiv h_{gc}(\omega_s^{(j)})$ within the resonance approximation yet less feasible. Thus, the theoretical problem is non-trivial.

Nevertheless, we show below in the self-consistent manner that, in the asymptotic limit $\Phi \rightarrow 0$, the frequency of egoscillation in the *whole* interval of relevant energies is close to ω_m and, moreover, the relevant boundaries of the

chaotic layers also lie in the range of energies E where $\omega(E) \approx \omega_m$. Therefore the resonant approximation is valid indeed and, ultimately, we shall obtain for $\omega_s^{(j)}$ and $h_s^{(j)}$ explicit asymptotic expressions.

So, let ω_f be close to an odd [23] n th harmonic of ω_m , $n \equiv (2j-1)$. For most of the energy interval $[E_b^{(1)}, E_b^{(2)}]$ except in the close vicinity of barriers levels, the n th harmonic of eigenoscillation is nearly resonant to the perturbation. Due to this, a slow dynamics of action $I \equiv I(E) = (2\pi)^{-1} \oint dq p$ and angle ψ [20] can be shown to be described by the following auxiliary Hamiltonian (cf. [1, 2, 3, 4, 5, 6]):

$$\begin{aligned}
\tilde{H}(I, \tilde{\psi}) &= \int_{I(E_m)}^I dI (n\omega - \omega_f) - nhq_n \cos(\tilde{\psi}) \\
&\equiv n(E - E_m) - \omega_f(I - I(E_m)) - nhq_n \cos(\tilde{\psi}), \\
I \equiv I(E) &= \int_{E_{\min}}^E \frac{d\tilde{E}}{\omega(\tilde{E})}, \quad E \equiv H_0(p, q), \\
\tilde{\psi} &= \psi - \omega_f t, \\
\psi &= \pi + \text{sgn}(p)\omega(E) \int_{q_{\min}(E)}^q \frac{d\tilde{q}}{\sqrt{2(E - U(\tilde{q}))}} + 2\pi l, \\
q_n \equiv q_n(E) &= \left| \frac{1}{2\pi} \int_0^{2\pi} d\psi q(E, \psi) \exp(in\psi) \right|, \\
n &= 1, 3, 5, \dots, \quad |n\omega - \omega_f| \ll \omega,
\end{aligned} \tag{4}$$

where E_{\min} is the minimal (over all q, p) energy $E \equiv H_0(p, q)$; $\omega \equiv \omega(E) = dH_0/dI$ and $q_{\min}(E)$ are respectively the frequency and the minimal coordinate of the conservative motion at a given value of energy E ; l is a number of right turning points in the trajectory $[q(\tau)]$ for the conservative motion with energy E and given initial coordinate q_0 and momentum p_0 .

Let us derive explicit expressions for various quantities in (4). In the unperturbed case ($h = 0$), the equations of motion (2) with H_0 (1) can be solved explicitly. Using their solution, one can find the explicit formula for $\omega(E)$:

$$\begin{aligned}
\omega(E) &= \frac{\pi(2E)^{1/4}}{2K[k]}, \\
k &= \frac{1}{2} \sqrt{\frac{(\sqrt{2E} + 1)^2 - \Phi^2}{\sqrt{2E}}},
\end{aligned} \tag{5}$$

where

$$K[k] = \int_0^{\frac{\pi}{2}} \frac{d\phi}{\sqrt{1 - k^2 \sin^2(\phi)}}, \tag{6}$$

is a full elliptic integral of the first order [24]. Using the asymptotic expression for $K[k]$,

$$K[k \rightarrow 1] \simeq \frac{1}{2} \ln \left(\frac{16}{1 - k^2} \right),$$

one obtains from (5), (6) the following expression for $\omega(E)$ in the asymptotic limit $\Phi \rightarrow 0$:

$$\begin{aligned}
\omega(E) &\simeq \frac{\pi}{\ln \left(\frac{64}{(\Phi - \Delta E)(\Phi + \Delta E)} \right)}, \\
\Delta E &\equiv E - \frac{1}{2}, \quad |\Delta E| < \Phi, \\
\Phi &\rightarrow 0.
\end{aligned} \tag{7}$$

The function $\omega(E)$ (7) is close to its maximum

$$\omega_m \equiv \max_{[E_b^{(1)}, E_b^{(2)}]} \{\omega(E)\} \simeq \frac{\pi}{2 \ln(8/\Phi)} \quad (8)$$

in the most of the interbarrier [25] range of energies $[1/2 - \Phi, 1/2 + \Phi]$, except the close vicinity of the barriers where either $|\ln(1/(1 - \Delta E/\Phi))|$ or $|\ln(1/(1 + \Delta E/\Phi))|$ becomes comparable with or larger than $\ln(8/\Phi)$ and therefore $\omega(E)$ sharply decreases to zero as $|\Delta E| \rightarrow \Phi$. The width of the aforementioned vicinity is $\sim \Phi^2$. Therefore its ratio to the whole interbarrier range ($2\Phi^2$) is $\sim \Phi$ i.e. goes to zero in the asymptotic limit $\Phi \rightarrow 0$: in other words, $\omega(E)$ approaches the *rectangular* form. As it will be clear from the further consideration, *it is this latter property that gives rise to the most characteristic features of the onset of global chaos in the system with two or more separatrices.*

One more quantity whose asymptotic expression will be used in the calculation (ω_s, h_s) is the Fourier harmonic $q_n \equiv q_n(E)$. The system stays most of the time very close to one of the barriers. Consider a motion within one of the periods of the periodic potential $U(q)$, namely in between neighboring upper barriers $[q_{ub}^{(1)}, q_{ub}^{(2)}]$ where $q_{ub}^{(2)} \equiv q_{ub}^{(1)} + 2\pi$. If energy $E \equiv 1/2 + \Delta E$ lies in the relevant range $[E_b^{(1)}, E_b^{(2)}]$, then the system stays close to the lower barrier $q_{lb} \equiv q_{ub}^{(1)} + \pi$ for the time [26]

$$T_l \approx 2 \ln \left(\frac{1}{\Phi + \Delta E} \right) \quad (9)$$

during each period of eigenoscillation, while it stays close to one of the upper barriers $q_{ub}^{(1,2)} \equiv q_{lb} \pm \pi$ for the most of the rest of the period of the eigenoscillation,

$$T_u \approx 2 \ln \left(\frac{1}{\Phi - \Delta E} \right) \quad . \quad (10)$$

Therefore, the function $q(E, \psi) - q_{lb}$ may be approximated by the following piecewise odd periodic function:

$$\begin{aligned} q(E, \psi) - q_{lb} &= \begin{cases} 0 & \text{at } \psi \in [0, \frac{\pi}{2} \frac{T_l}{T_l + T_u}] \cup [\pi - \frac{\pi}{2} \frac{T_l}{T_l + T_u}, \pi], \\ \pi & \text{at } \psi \in [\frac{\pi}{2} \frac{T_l}{T_l + T_u}, \pi - \frac{\pi}{2} \frac{T_l}{T_l + T_u}], \end{cases} \\ q(E, -\psi) - q_{lb} &= -(q(E, \psi) - q_{lb}), \\ q(E, \psi \pm 2\pi j) &= q(E, \psi), \\ j &= 1, 2, 3, \dots \end{aligned}$$

Substituting the above approximation of $q(E, \psi)$ into the definition of q_n (4), one can obtain:

$$\begin{aligned} q_{2j-1} &\equiv q_{2j-1}(E) = \frac{2}{2j-1} \cos \left[\frac{\pi/2}{1 + \frac{\ln(\frac{1}{\Phi - \Delta E})}{\ln(\frac{1}{\Phi + \Delta E})}} \right], \\ \Phi &\rightarrow 0, \\ q_{2j} &= 0, \\ j &= 1, 2, 3, \dots \end{aligned} \quad (11)$$

It follows from (11) that $q_{2j-1}(E)$ monotonously increases in the interval $E \in [E_b^{(1)}, E_b^{(2)}]$ from the minimum at $E = E_b^{(1)}$

$$q_{2j-1}(E_b^{(1)}) = 0$$

to the maximum at $E = E_b^{(2)}$

$$q_{2j-1}(E_b^{(2)}) = \frac{2}{(2j-1)}.$$

But this increase occurs mostly in the close vicinity of the barriers while, in the major part of the interval $[E_b^{(1)}, E_b^{(2)}]$ the argument of the cosine in Eq.(11) is close to $\pi/4$ and q_{2j-1} is almost constant:

$$q_{2j-1} \approx \frac{\sqrt{2}}{2^j - 1}, \quad j = 1, 2, 3, \dots, \quad (12)$$

$$\left| \ln \left(\frac{1 + \Delta E/\Phi}{1 - \Delta E/\Phi} \right) \right| \ll 2 \ln \left(\frac{1}{\Phi} \right).$$

The inequality in (12) determines the range of ΔE where the approximate equality (12) for q_{2j-1} is valid. In the asymptotic limit $\Phi \rightarrow 0$, this range includes almost the whole interval $]-\Phi, \Phi[$.

Apart from $\omega(E)$ and $q_n(E)$, we shall need also the asymptotic expression of action I via energy E . Substituting $\omega(E)$ (7) into the definition of $I(E)$ (4) and carrying out the integration in this definition in an explicit form, one obtains

$$I(E) = I(1/2) + \frac{\Delta E \ln \left(\frac{64e^2}{\Phi^2 - (\Delta E)^2} \right) + \Phi \ln \left(\frac{\Phi - \Delta E}{\Phi + \Delta E} \right)}{\pi},$$

$$\Phi \rightarrow 0. \quad (13)$$

Let us turn to the analysis of the *dynamics* of the auxiliary Hamiltonian system (4). Our goal is to find the *separatrix* which satisfies two following conditions.

- It should include one or more hyperbolic unstable stationary points, often called *saddles* [1, 2, 3, 4]. The motion near a saddle is slowed down so that, for the full system (2)-(1), the fast-oscillating terms neglected in (4) give rise to the thin chaotic layer around the separatrix of the system (4) [1, 2, 3, 4, 5, 6].
- For a given ω_f the separatrix should overlap both chaotic layers associated with the separatrices of the unperturbed system H_0 (1) provided that h exceeds the critical value $h_{gc}(\omega_f)$.

Equations of motion of the system (4) for a given odd n and for the relevant range of frequency ω_f (i.e. $\omega_f \approx n\omega_m$) read as:

$$\dot{I} = -\frac{\partial \tilde{H}}{\partial \tilde{\psi}} \equiv -nhq_n \sin(\tilde{\psi}), \quad (14)$$

$$\dot{\tilde{\psi}} = \frac{\partial \tilde{H}}{\partial I} \equiv n\omega - \omega_f - nh \frac{dq_n}{dI} \cos(\tilde{\psi}).$$

The system (14) may have up to 8 stationary points per 2π interval of $\tilde{\psi}$. Let us first exclude those of them which are definitely irrelevant to the separatrices satisfying the conditions described above. There are two unstable stationary points corresponding to $E = E_b^{(1)}$ (we remind that $q_n(E_b^{(1)}) = 0$) and $\tilde{\psi} = \pm\pi/2$. But there is no slowing down near these points and, therefore, they do not generate chaotic layers. Thus, these points are irrelevant in the context of our work. If $E \neq E_b^{(1)}$, then $q_n \neq 0$ and therefore the right-hand part of the first of equations (14) is equal to zero only if $\tilde{\psi}$ is equal either to 0 or to π . Substituting these values into the second of equations (14) and putting $\dot{\tilde{\psi}} = 0$, we obtain the equations for the corresponding actions:

$$X_{\mp}(I) \equiv n\omega - \omega_f \mp nhdq_n/dI = 0, \quad (15)$$

where the signs “-” and “+” correspond to $\tilde{\psi} = 0$ and $\tilde{\psi} = \pi$ respectively. A typical example of the graphic solution of equations (15) is shown in Fig. 9. Two of the roots corresponding to $\tilde{\psi} = \pi$ are very close to the values of I corresponding to the potential barriers (we remind that relevant values of h are small). These roots arise due to the divergence of dq/dI as E approaches the barriers. The lower/upper root corresponds to a stable/unstable point. However both these points as well as the separatrix generated by the unstable point lie in the ranges covered by the chaotic layers associated with the separatrices of the unperturbed system (see the Appendix). Therefore, they are also irrelevant to our search for independent chaotic layers.

Let us consider the stationary points corresponding to the remaining four roots of equations (15). As follows from the analysis of the equations (14) linearized near the stationary points (cf. [1, 2, 3, 4]), two of them are stable elliptic

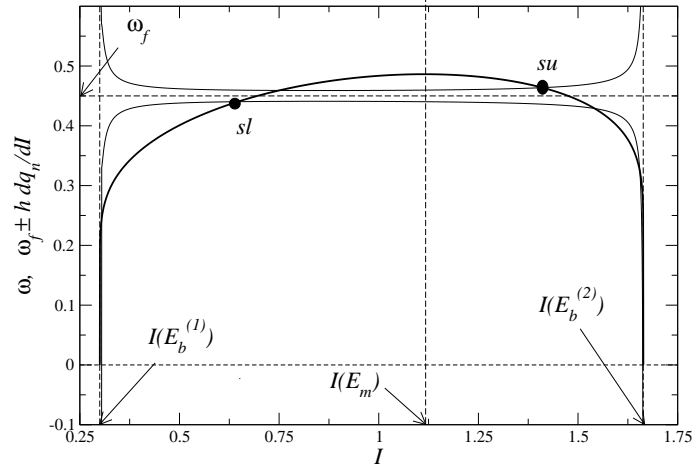


FIG. 9: A schematic example illustrating graphic solutions of equations (15) as intersections of the curve $\omega(I)$ (drawn by the thick solid line) with the curves $\omega_f \pm h dq_n(I)/dI$ for $n = 1$ (drawn by the thin solid lines). The solutions corresponding to the lower and upper relevant saddles (defined by Eq.(16)) are marked by dots and by the labels sl and su respectively (we do not mark other solutions because they are irrelevant).

points, often called *nonlinear resonances* [27], while two others are unstable hyperbolic points i.e. *saddles*. Just the latter saddles are of the major interest in the context of our work. They belong to the *separatrices* separating the regions of oscillations about the resonances from the regions of a motion with a “running” slow angle ψ . For the full system (2)-(1), these separatrices are “dressed” by chaotic layers which may provide the connection between chaotic layers associated with the barriers, thus leading to the onset of the global chaos.

We shall distinguish the relevant saddles as saddles with the *lower* action/energy (using the subscript “ sl ”) and *upper* action/energy (using the subscript “ su ”). The positions of the saddles in the $I - \tilde{\psi}$ plane are defined by the following equations (cf. Figs. 8 and 9):

$$\begin{aligned} \tilde{\psi}_{su} &= 0, & \tilde{\psi}_{sl} &= \pi, \\ X_+(I_{sl}) &= X_-(I_{su}) = 0, \\ \frac{dX_+(I_{sl})}{dI_{sl}} &> 0, & \frac{dX_-(I_{su})}{dI_{su}} &< 0, & I_{sl} < I_{su}, \end{aligned} \quad (16)$$

where $X_{\pm}(I)$ are defined in Eq. (15).

Given that values of h relevant to the minima of the spikes are small in the asymptotic limit $\Phi \rightarrow 0$, one may neglect in the lowest-order approximation the last term in the definition of X_{\mp} in Eq. (15) [28] so that the equations $X_{\mp} = 0$ reduce to the simple resonance condition

$$n\omega(I_{su,sl}) = \omega_f. \quad (17)$$

Substituting here Eq. (7) for ω , one obtains the explicit expressions for energies in the saddles:

$$\begin{aligned} E_{su,sl} &\approx \frac{1}{2} \pm \Delta E^{(1)}, \\ \Delta E^{(1)} &\equiv \sqrt{\Phi^2 - 64 \exp\left(-\frac{n\pi}{\omega_f}\right)}, \\ \omega_f &\leq n\omega_m. \end{aligned} \quad (18)$$

The corresponding actions $I_{su,sl}$ are expressed via $E_{su,sl}$ by means of Eq. (13).

Assuming that the relevant frequency ω_f is close to $n\omega_m$, it follows from (18) that the values of $E_{su,sl}$ lie in the range where the expression (12) for q_n does hold true. This will obviously be confirmed in the end by the results of calculations based on this assumption.

Using (16) for the angles and (18) for the energies as well as the asymptotic expressions (7), (12) and (13) for $\omega(E)$, $q_n(E)$ and $I(E)$ respectively and allowing for the resonance condition (17), one obtains explicit expressions for the values of the Hamiltonian (4) in the saddles:

$$\tilde{H}_{sl} = -\tilde{H}_{su} = \frac{\omega_f}{\pi} \left[2\Delta E^{(1)} - \Phi \ln \left(\frac{\Phi + \Delta E^{(1)}}{\Phi - \Delta E^{(1)}} \right) \right] + h\sqrt{2}. \quad (19)$$

As explained above, one of the two major conditions which should be satisfied in the spikes is the reconnection in the phase space between the chaotic layers surrounding nonlinear resonances. The latter is well approximated by the *separatrix reconnection* [4, 5, 6] in the resonance approximation. The separatrix reconnection marks the so called ZDNR/NR transition [4] when the topology of the resonance separatrices changes from the ZDNR type [4, 5, 6] to the conventional NR one [1, 2, 3]: cf. Fig. 3 or Fig. 8. Given that a value of the Hamiltonian function \tilde{H} does not change along any trajectory of the system (4) (in particular, along any of the separatrices), the lower and upper saddles on the *reconnected* separatrices should possess equal values of \tilde{H} :

$$\tilde{H}_{sl} = \tilde{H}_{su}, \quad (20)$$

that may be considered as the necessary condition for the reconnection.

Taking into account that $\tilde{H}_{sl} = -\tilde{H}_{su}$ (see (19)), it follows from (20) that

$$\tilde{H}_{sl} = \tilde{H}_{su} = 0. \quad (21)$$

In the explicit form, both relations in (21) reduce to the following one:

$$\begin{aligned} h &\equiv h(\omega_f) = \frac{\omega_f}{\sqrt{2}\pi} \left[\Phi \ln \left(\frac{\Phi + \Delta E^{(1)}}{\Phi - \Delta E^{(1)}} \right) - 2\Delta E^{(1)} \right], \\ \Delta E^{(1)} &\equiv \sqrt{\Phi^2 - 64 \exp\left(-\frac{n\pi}{\omega_f}\right)}, \\ 0 < \omega_m - \omega_f/n &\ll \omega_m \equiv \frac{\pi}{2 \ln(8/\Phi)}, \\ n &= 1, 3, 5, \dots \end{aligned} \quad (22)$$

The function $h(\omega_f)$ described by Eq.(22) monotonously decreases to zero as ω_f grows from 0 to $n\omega_m$, where the line abruptly.

The next step is to find the minimal possible h at which the reconnected separatrices overlap both chaotic layers related to the potential barriers levels. In order to do this, one has to know how the relevant outer boundaries of the chaotic layers behave as h and ω_f vary. If to assume that the relevant ω_f is close to $n\omega_m$ while the relevant h is sufficiently large for $\omega(E)$ to be close to ω_m at any point of the outer boundaries of the layers (the results should confirm these assumptions), then the motion on the regular trajectories that are infinitesimally close to the layer boundaries may be described within the resonance approximation. Therefore the boundaries may also be described as trajectories of the auxiliary resonant Hamiltonian system (4). It is shown in the Appendix that, unless h exceeds some critical value $h_{cr}^{(l)}(\omega_f)$ (this value is determined by Eq. (27) below), the upper boundary of the lower layer is formed by the trajectory of the system (4) that includes the states

$$\begin{aligned} \tilde{\psi} &= 2\pi m, \quad m = 0, \pm 1, \pm 2, \dots, \\ I &= I(E = E_b^{(1)} + \delta_l), \end{aligned} \quad (23)$$

where δ_l is the so called *separatrix split* [29] for the lower layer and is approximated in the lowest order in Φ as

$$\delta_l = \sqrt{2}\pi h \quad (24)$$

(a more accurate expression for δ_l/h is given in Eq. (A11)). But, if $h > h_{cr}^{(l)}(\omega_f)$, then each such trajectory lies inside one of the loops of the separatrix of the lower nonlinear resonance. In the latter case, such a trajectory typically forms

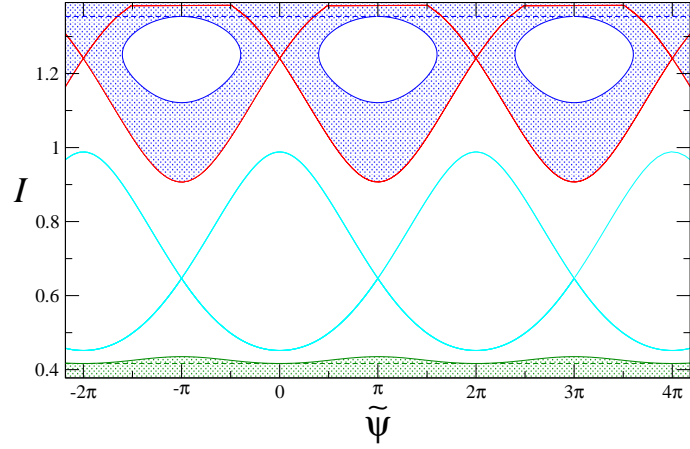


FIG. 10: Example of the theoretically calculated boundaries of the chaotic layers (shaded in green and blue, for the upper and lower layers respectively). The parameters are the same as in Figs. 7(b) and Fig. 8(b). The barriers levels of I coincide with the lower and upper boundaries of the figure box. The resonance separatrices are drawn by the magenta and red solid lines (for the lower and upper resonances respectively). The dashed green and blue lines mark the levels corresponding to $E = E_b^{(1)} + \delta_l$ and $E = E_b^{(2)} - \delta_u$ respectively, where δ_l and δ_u are the values of the separatrix split for the lower and upper barrier respectively. The upper boundary of the lower layer is formed by the trajectory of the auxiliary resonant Hamiltonian system (4) that includes the state $(I = I(E = E_b^{(1)} + \delta_l), \tilde{\psi} = 0)$. The lower boundary of the upper layer is formed by the lower part of the upper (red) resonance separatrix. The periodic closed loops (solid blue lines) are the trajectories of the system (4) that start from the states $(I = I(E = E_b^{(2)} - \delta_u), \tilde{\psi} = \pi + 2\pi m)$ where m is any integer: they form the boundaries of the major stability islands inside the upper chaotic layer.

only the boundary of the major stability island inside the lower chaotic layer (repeated periodically in $\tilde{\psi}$), while the upper boundary of the layer is formed by the upper part of the resonance separatrix. This may be interpreted as the absorption (overlap) of the lower resonance by the lower chaotic layer.

Similarly, unless h exceeds some critical value $h_{cr}^{(u)}(\omega_f)$ (this value is determined by Eq. (28) below), the lower boundary of the upper chaotic layer is formed by the trajectory of the system (4) that includes the states

$$\begin{aligned} \tilde{\psi} &= \pi + 2\pi m, & m &= 0, \pm 1, \pm 2, \dots, \\ I &= I(E = E_b^{(2)} - \delta_u), \end{aligned} \quad (25)$$

where the lowest-order approximation for the upper separatrix split δ_u reads as

$$\delta_u = \sqrt{2\pi}h \quad (26)$$

(a more accurate expression for δ_u/h is given by Eq. (A25)). But, if $h > h_{cr}^{(u)}(\omega_f)$, then each such trajectory lies inside one of the loops of the separatrix of the upper nonlinear resonance. In the latter case, such a trajectory typically forms only the boundary of the major stability islands inside the upper chaotic layer (repeated periodically in $\tilde{\psi}$), while the lower boundary of the layer is formed by the lower part of the resonance separatrix. This may be interpreted as the absorption (overlap) of the upper resonance by the upper chaotic layer.

The description of the layers boundaries given above is illustrated by Fig. 10 (it relates to the same values of h and ω_f as those for Fig. 7(b)). One concludes from Fig. 10 that, for the given values of h and ω_f , the theory predicts the following features: (i) the lower chaotic layer does not overlap the lower resonance but is quite close to it, (ii) the upper layer overlaps (absorbs) the upper resonance; at the same time, the resonance is still manifested in the form of large stability islands inside the layer, (iii) the upper layer is not reconnected with the lower resonance. All these theoretical predictions agree with the Poincare section of the original system (Fig. 7(b)).

The description of the chaotic layers given above and, in more details, in the Appendix is the first major result of the present paper. It provides for the *rigorous base* for our intuitive assumption that the minimal value of h at which the layers overlap should correspond to the reconnection of the nonlinear resonances with each other while the reconnected resonances touch one of the layers and touch/overlap the another one. It is remarkable also that we have managed to obtain the *quantitative* theoretical description of the chaotic layers boundaries in the *phase space*, including even the major stability islands.

The condition for the separatrix of the lower resonance to touch the lower chaotic layer may be written as

$$\tilde{H}(I = I(E = E_b^{(1)} + \delta_l), \tilde{\psi} = 0) = \tilde{H}_{sl}. \quad (27)$$

Similarly, the condition for the separatrix of the upper resonance to touch the upper chaotic layer is

$$\tilde{H}(I = I(E = E_b^{(2)} - \delta_u), \tilde{\psi} = \pi) = \tilde{H}_{su}. \quad (28)$$

Either of Eqs. (27) and (28) should be combined with the condition of the separatrix reconnection (20). If to restrict ourselves to the obtaining only the leading terms of $h_s \equiv h_s(\Phi)$ and $\omega_s \equiv \omega_s(\Phi)$, then the exact relation (20) may be replaced by its lowest-order approximation (21) or by the equivalent to it Eq. (22). Using also the approximate expressions for the barriers ($E_b^{(1,2)} \approx 1/2 \mp \Phi$), Eqs. (27) and (28) may be written in the approximate form respectively as

$$\tilde{H}(I = I(E = 1/2 - \Phi + \delta_l), \tilde{\psi} = 0) = 0, \quad (29)$$

and

$$\tilde{H}(I = I(E = 1/2 + \Phi - \delta_u), \tilde{\psi} = \pi) = 0, \quad (30)$$

where $\delta_{l,u} \approx \sqrt{2\pi}h$ as follows from (24) and (26). Before to move on, we comment that we keep the separatrix splits $\delta_{l,u}$ in these equations in a semi-implicit form - in order to explicitly demonstrate below that $\delta_{l,u}$ do not affect the leading term of h_s (and, even more so, of ω_s). The physical reason for such an independence of the leading term of h_s is that, unlike the case of the conventional separatrix layer, the separatrix split determines in our case just the *minimal* (rather than maximal) deviation of the layer boundary from the barrier level while the maximal deviation ($\sim \Phi$) is logarithmically larger.

Strictly speaking, the solution ($h_s^{(l)}, \omega_s^{(l)}$) of the system of equations (22),(29) may differ from the solution ($h_s^{(u)}, \omega_s^{(u)}$) of the system of equations (22),(30). Therefore, after each of the solutions is obtained, it is necessary to check whether the solution ($h_s^{(l)}, \omega_s^{(l)}$) provides for the overlap of the resonances with the upper chaotic layer and whether the solution ($h_s^{(u)}, \omega_s^{(u)}$) provides for the overlap of the resonances with the lower chaotic layer. It turns out that the *leading* terms of the solutions are *identical*. If to take into account the higher-order terms, one may show that the solution ($h_s^{(l)}, \omega_s^{(l)}$) does provide for the overlap with the upper chaotic layer whilst the solution ($h_s^{(u)}, \omega_s^{(u)}$) does not provide for the overlap with the lower chaotic layer (which agrees with the evolution of the Poincaré section: cf. Fig. 7). Thus, the solution ($h_s^{(l)}, \omega_s^{(l)}$) may be identified as the minimum of the spike (h_s, ω_s) anyway.

The system of algebraic equations (22) and (29) is still too complicated to find its exact solution. But we may restrict ourselves to the search for the *asymptotic* solution. Still, even this simplified problem is not trivial, both because the function $h_s(\Phi)$ turns out non-analytic and because $\Delta E^{(1)}$ in (22) is very sensitive to ω_f in the relevant range. Despite these difficulties, we have managed to find the solution in the *self-consistent* manner, i.e. we have made some reasonable assumption about the functional dependence $h_s(\Phi)$ while the result obtained on the base of this assumption and of the earlier assumption for ω_s to approach ω_m as $\Phi \rightarrow 0$ has confirmed both these assumptions. Details are presented below.

So, let us assume that the asymptotic dependence $h_s(\Phi)$ reads as:

$$h_s = a \frac{\Phi}{\ln(4e/\Phi)}, \quad (31)$$

where the unknown constant multiplier a is to be found from the solution of (22), (29), (31) with the asymptotic limit $\Phi \rightarrow 0$ being taken into account. Substituting the energies $E = 1/2 - \Phi + \delta_l$ and $E = 1/2 + \Phi - \delta_u$ into the formula (7) and taking into account (24), (26) and (31), we find that the inequality

$$\omega_m - \omega(E) \ll \omega_m \quad (32)$$

holds in the whole relevant interval of energies, i.e. for

$$\Delta E \in [-\Phi + \delta_l, \Phi - \delta_u]. \quad (33)$$

Thus, the resonant approximation is valid in the whole relevant interval (33). Besides, it follows from (24), (26) and (31) that Eq. (12) for $q_n(E)$ is valid in the whole relevant interval of energies too.

Let us consider Eq. (29) in a more explicit form. Namely, let us express ω_f from Eq.(29), using Eqs. (4), (12), and (13):

$$\begin{aligned} \omega_f = & \frac{n\pi}{2 \ln\left(\frac{4e}{\Phi}\right)} \left[1 + \frac{h\sqrt{2}}{n\Phi} - \frac{\delta_l}{2\Phi} \frac{\ln\left(\frac{e\delta_l}{2\Phi}\right)}{\ln\left(\frac{4e}{\Phi}\right)} \right] + \\ & + O\left(1/\ln^2\left(\frac{4e}{\Phi}\right)\right), \end{aligned} \quad (34)$$

where δ_l is given by (24) while the last term $O(1/\ln^2(4e/\Phi))$ allows for (24) and (31). Note that, despite it is formally not essential to keep the numerical constants like 4 or e in the arguments of the logarithms in the asymptotic limit $\Phi \rightarrow 0$, we do keep them in (34) in order to keep a satisfactory accuracy of the theory in case of moderately (rather than extremely) small Φ : the asymptotic expansion converges *slowly* since the divergence of the logarithmic function $\ln(x \rightarrow 0)$ is slow.

We substitute (34) into the expression for $\Delta E^{(1)}$ in (22) and, using (31) and the identity

$$x^{\frac{y}{\ln(1/x)}} \equiv e^{-y}, \quad (35)$$

as well as the asymptotic relation

$$\delta_l/\Phi \xrightarrow{\Phi \rightarrow 0} 0 \quad (36)$$

(that follows from (24) and (31)), and neglecting corrections vanishing in the asymptotic limit $\Phi \rightarrow 0$ (this concerns in particular the term related to δ_l), we obtain

$$\begin{aligned} \Delta E^{(1)} &= \Phi \sqrt{1 - 4e^{c-2}}, \\ c &\equiv \frac{2\sqrt{2}}{n} a. \end{aligned} \quad (37)$$

Substituting $\Delta E^{(1)}$ from (37) into Eq. (22) for $h(\omega_f)$ and allowing for (31) once again, we arrive at the transcendental equation for c :

$$\begin{aligned} \ln\left(\frac{1 + \chi(c)}{1 - \chi(c)}\right) - 2\chi(c) &= c, \\ \chi(c) &\equiv \sqrt{1 - 4e^{c-2}}. \end{aligned} \quad (38)$$

The approximate numerical solution of (38) is:

$$c \simeq 0.179 \dots \quad (39)$$

Thus, the final leading-order asymptotic formulas for ω_f and h in the minima of the spikes are the following:

$$\begin{aligned} \omega_{s0} &\equiv \omega_{s0}^{\left(\frac{n+1}{2}\right)} = n \frac{\pi}{2 \ln\left(\frac{4e}{\Phi}\right)}, \\ h_{s0} &\equiv h_{s0}^{\left(\frac{n+1}{2}\right)} = n \frac{c}{2\sqrt{2}} \frac{\Phi}{\ln\left(\frac{4e}{\Phi}\right)}, \\ n &= 1, 3, 5, \dots, \\ \Phi &\rightarrow 0, \end{aligned} \quad (40)$$

where the constant $c \approx 0.179$ is the solution of Eq. (38).

The rigorous derivation of the explicit asymptotic formulas for the minima of $h_{gc}(\omega_f)$ is the second major result of the paper. These formulas allow to immediately predict parameters of the weakest driving which may lead to the global chaos.

For $\Phi = 0.2$, the numerical simulations give the following values for the frequencies in the minima of the first two spikes (see Fig. 6):

$$\omega_s^{(1)} \approx 0.400 \div 0.401, \quad \omega_s^{(2)} \approx 1.23 \div 1.25. \quad (41)$$

The values by the lowest-order formula (40) are:

$$\omega_{s0}^{(1)} \approx 0.393, \quad \omega_{s0}^{(2)} \approx 1.18, \quad (42)$$

quite well agreeing with the simulations.

For h in the spikes minima, the simulations give the following [30] values (see Fig. 6):

$$h_s^{(1)} \approx 0.0048, \quad h_s^{(2)} \approx 0.03. \quad (43)$$

The values by the lowest-order formula (40) are:

$$h_{s0}^{(1)} \approx 0.0032, \quad h_{s0}^{(2)} \approx 0.01. \quad (44)$$

The theoretical value $h_{s0}^{(1)}$ gives a reasonable estimate for the simulation value $h_s^{(1)}$. The theoretical value $h_{s0}^{(2)}$ gives a correct order of magnitude for the simulation value $h_s^{(2)}$. The accuracy of the formula (40) for h_s is much lower than that for ω_s , which is due to the steepness of $h_{gc}(\omega_f)$ in the ranges of spikes. The latter, in turn, is due to the flatness of the function $\omega(E)$ near its maximum.

The next-order correction for ω_s can be immediately found from Eq. (34) for ω_f and Eq. (40) for h_{s0} :

$$\omega_{s1} \simeq \omega_{s0} \left(1 + \frac{c}{2 \ln\left(\frac{4e}{\Phi}\right)} \right) \approx \frac{n\pi \left(1 + \frac{0.09}{\ln\left(\frac{4e}{\Phi}\right)} \right)}{\ln\left(\frac{4e}{\Phi}\right)}, \quad (45)$$

$n = 1, 3, 5, \dots$

The formula (45) agrees with the simulations yet better than the lowest-order approximation:

$$\omega_{s1}^{(1)} \approx 0.402, \quad \omega_{s1}^{(2)} \approx 1.21. \quad (46)$$

The next-order correction for h_s is of the order of $\ln[\ln(1/\Phi)]/\ln(1/\Phi)$: it originates from the non-zero value of δ_l and can be found in a manner similar to that used for the derivation h_{s0} . Namely we assume that, instead of (31), the following relation holds true:

$$h_s = h_{s0} \left(1 + b \frac{\ln[\ln(4e/\Phi)]}{\ln(4e/\Phi)} \right) \quad (47)$$

with the unknown constant b . Solving the system of equations (22), (29) and (47) in the manner similar to that described above and omitting corrections of the order of $1/\ln(1/\Phi)$, we obtain:

$$\begin{aligned} h_{s1} &= h_{s0} \left(1 - n \frac{\pi \sqrt{1 - 4e^{c-2}}}{2(1 + \sqrt{1 - 4e^{c-2}})} \frac{\ln[\ln(4e/\Phi)]}{\ln(4e/\Phi)} \right) \\ &\approx h_{s0} \left(1 - 0.585n \frac{\ln[\ln(4e/\Phi)]}{\ln(4e/\Phi)} \right). \end{aligned} \quad (48)$$

It gives for the first two spikes:

$$h_{s1}^{(1)} \approx 0.0026, \quad h_{s1}^{(2)} \approx 0.004. \quad (49)$$

These values differ from the simulation values (43) even more than the lowest-order values (44). This means that, for the given *moderately* small value of Φ , the correction of the yet more high order (i.e. $\propto 1/\ln(1/\Phi)$) has the different sign and the larger value, in comparison with the correction of the formally lower order (i.e. $\propto \ln[\ln(1/\Phi)]/\ln(1/\Phi)$) [31]. However, the consistent derivation of the former correction in an explicit form is very complicated. As a reasonable alternative, one may seek the proper *numerical* solution of the algebraic system of Eqs. (20) and (27) [32]. To do this, one has to use in Eqs. (20) and (27): (i) the exact values of saddle energies obtained from the exact relations (16) instead of the simplified resonance conditions (17); (ii) the exact formulas (5) and (6) for $\omega(E)$ instead of the asymptotic expression (7); (iii) the exact functions $q_n(E)$ instead of the asymptotic formula (12); (iv) the more accurate than (24) estimate for δ_i/h by (A11). Note that, to find the exact function $q_n(E)$, we substitute the explicit solution for $q(E, \psi)$ into the definition (4) of $q_n(E)$ [34]:

$$\begin{aligned} q(E, \psi) &= \arcsin\left(\frac{\eta - \sqrt{2E} + \Phi}{1 - \eta}\right) & \text{for } \psi \in \left[0, \frac{\pi}{2}\right], \\ q(E, \psi) &= \pi - q(E, \pi - \psi) & \text{for } \psi \in \left[\frac{\pi}{2}, \pi\right], \\ q(E, \psi) &= q(E, 2\pi - \psi) & \text{for } \psi \in [\pi, 2\pi], \\ \eta &\equiv \frac{1}{2}(\sqrt{2E} - \Phi + 1)\text{sn}^2\left(\frac{2K}{\pi}\psi\right), \end{aligned} \quad (50)$$

where $\text{sn}(x)$ is an elliptic sine [24] with the same modulus k as for the full elliptic integral K defined in (5),(6).

For the first spike, the numerical solution described above gives:

$$\omega_{sn}^{(1)} \approx 0.403, \quad h_{sn}^{(1)} \approx 0.0044. \quad (51)$$

The agreement of $h_{sn}^{(1)}$ with the simulation is much better in comparison with the lowest-order formula (40) (and yet more so with the formula (48)). Thus, if Φ is just moderately small while one needs to make a more accurate prediction for h_s than that one by the lowest-order formula, then the numerical procedure may be used.

IV. THEORETICAL DESCRIPTION OF THE WINGS OF THE SPIKES

Apart from the very minima of the spikes, it is important to understand mechanisms responsible for the formation of their *wings*, i.e. of the function $h_{gc}(\omega_f)$ in the ranges of ω_f deviating from $\omega_s^{(j)}$, and to provide for a quantitative theoretical description of the wings.

Before to develop the theory, we briefly analyse the simulation data (Fig. 6), concentrating on the 1st spike. The left wing of the spike is rather smooth nearly straight line. The initial part of the right wing is also nearly straight [35], though less steep, line. But, at some rather small distance from $\omega_s^{(1)}$, its slope changes jump-wise by a few times: compare the derivative [35] $dh_{gc}/d\omega_f \approx 0.1$ at ω_f just slightly exceeding $\omega_s^{(1)} \approx 0.4$ (see the left inset in Fig. 6) and $dh_{gc}/d\omega_f \approx 0.4$ at $\omega_f = 0.45 \div 0.55$ (see Fig. 6). Thus, even prior the theoretical analysis one may assume that there are a few different major mechanisms responsible for the formation of the spike wings.

Consider now an arbitrary j th spike. We have shown in the previous section that the minimum of the spike corresponds to the intersection of the separatrix reconnection line, given by Eq. (20), and of the line given by Eq. (27). We remind that Eq. (20) corresponds to the overlap in the phase space between nonlinear resonances of the same order $n \equiv 2j - 1$ while Eq. (27) corresponds to the onset of the overlap between the resonance separatrix associated with the lower saddle and the chaotic layer associated with the lower potential barrier. Note also that, for $\omega_f = \omega_s^{(j)}$, the condition (27) guarantees also the overlap between the upper resonance separatrix and the chaotic layer associated with the upper barrier.

If ω_f becomes smaller than $\omega_s^{(j)}$ the resonances shift closer to the barriers while separating from each other. Hence, as h increases, the overlap of the resonances with the chaotic layers associated with the barriers occurs earlier than with each other. Therefore, at $0 < \omega_s^{(j)} - \omega_f \ll \omega_m$, the function $h_{gc}(\omega_f)$ should approximately correspond just to the

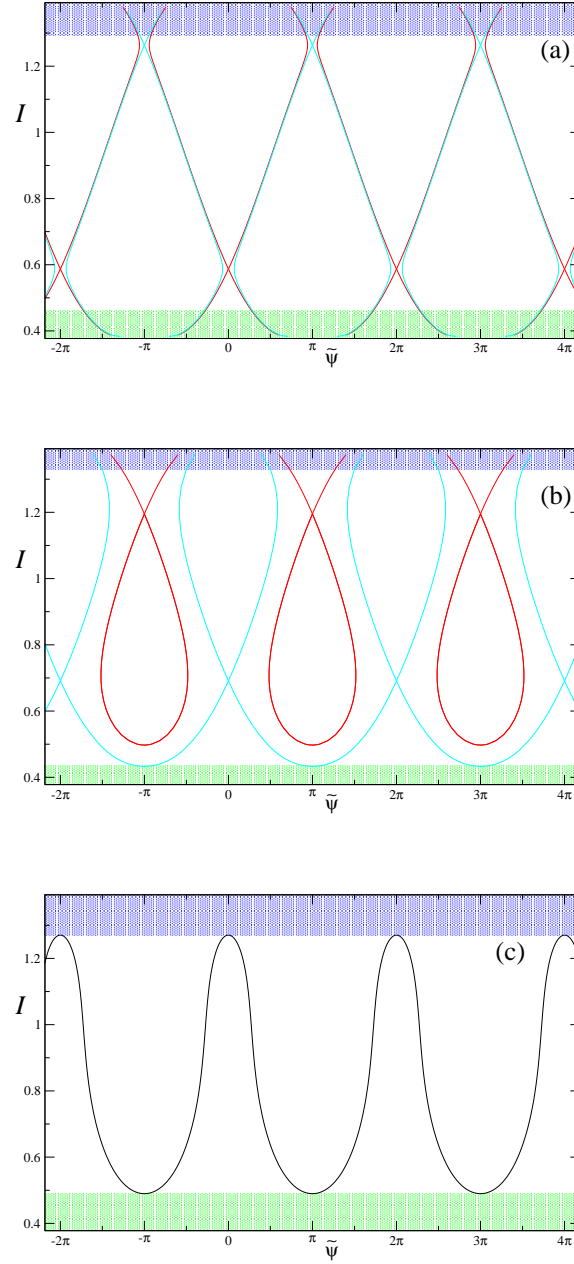


FIG. 11: Semi-schematic illustrations to the mechanisms of the formation of the spikes wings and to the corresponding theoretical lines in Fig. 12. Boxes (a), (b) and (c) illustrate the lines by Eqs. (20), (27) and (55) respectively: the corresponding perturbation parameters are $(\omega_f = 0.39, h = 0.08)$, $(\omega_f = 0.41, h = 0.05)$ and $(\omega_f = 0.43, h = 0.077)$ respectively. Resonance separatrices are drawn by red and magenta. The upper boundary of a green shaded strip and the lower boundary of a blue shaded strip indicate in each box the corresponding separatrix split levels for the lower and upper separatrices respectively i.e. levels of I corresponding to energies $(E_b^{(1)} + \delta_l)$ and $(E_b^{(2)} - \delta_u)$ respectively. The black line in (c) is the trajectory of the resonant Hamiltonian system (4) that touches both separatrix split levels.

reconnection of resonances of the order $n \equiv 2j - 1$ (Fig. 11(a)). Fig. 12 demonstrates that even the asymptotic formula (22) for the separatrix reconnection line fits the left wing of the spike quite well while the numerically calculated line (20) agrees with the simulations really perfectly [36].

If ω_f becomes slightly larger than $\omega_s^{(j)}$ then, on the contrary, the resonances shift closer to each other and more far from the barriers. Therefore, the overlap of resonances with each other occurs at smaller h than the overlap between

any of them and the chaotic layer associated with the lower barrier (cf. Figs. 7(c) and 7(d) as well as 8(c) and 8(d)). Hence, just the latter overlap determines the function $h_{gc}(\omega_f)$ in the relevant range of ω_f (Fig. 11(b)). Fig. 12 shows that $h_{gc}(\omega_f)$ is indeed well approximated in the close vicinity to the right from $\omega_s^{(1)}$ by the numerically solved Eq. (27) and, even, by its asymptotic form [37],

$$\begin{aligned} h &\equiv h(\omega_f) = & (52) \\ &\frac{-\Phi + \frac{\omega_f}{n\pi} \left[\Phi \left\{ 2 \ln \left(\frac{4e}{\Phi} \right) + \ln \left(\frac{\Phi + \Delta E^{(1)}}{\Phi - \Delta E^{(1)}} \right) \right\} - 2\Delta E^{(1)} \right]}{2\sqrt{2}}, \\ n &\equiv 2j - 1, \quad |\omega_f - \omega_s^{(j)}| \ll \omega_m, \end{aligned}$$

where $\Delta E^{(1)} \equiv \Delta E^{(1)}(\omega_f)$ is the smaller of the two positive roots of the equation

$$\frac{\omega_f}{n\pi} \ln \left(\frac{64}{\Phi^2 - (\Delta E^{(1)})^2} \right) - 1 - hq'_n = 0, \quad (53)$$

where h is to be expressed by means of Eq. (50) while q'_n is the derivative of the asymptotic function q_n (11) with respect to E in which, after the differentiation, ΔE is replaced by $\Delta E^{(1)}$, i.e.

$$\begin{aligned} q'_n &= \frac{\pi}{n} \sin \left[\frac{\pi/2}{1 + \mu_1/\mu_2} \right] \frac{\frac{\mu_1}{\Phi - \Delta E^{(1)}} + \frac{\mu_2}{\Phi + \Delta E^{(1)}}}{(\mu_1 + \mu_2)^2}, & (54) \\ \mu_{1,2} &\equiv \ln \left(\frac{1}{\Phi \pm \Delta E^{(1)}} \right). \end{aligned}$$

The above mechanism determines $h_{gc}(\omega_f)$ only in the close vicinity of $\omega_s^{(j)}$. If ω_f/n becomes too close to ω_m or exceeds it, then the resonances are not of an immediate relevance: they may even not exist or, if they still exist, their closed loops shrink, so that they cannot anymore provide for the connection of the chaotic layers in the relevant range of h . At the same time, the closeness of the frequency to ω_m still gives rise to a large variation of action along many of the trajectories of the resonant Hamiltonian system (4). As explained in the Appendix, the boundaries of the chaotic layers are formed in this case just by the trajectories of (4) which start in the states ($I = I(E = E_b^{(1)} + \delta_l), \tilde{\psi} = 0$) or ($I = I(E = E_b^{(2)} - \delta_u), \tilde{\psi} = \pi$), for the lower and the upper layers respectively. Obviously, the overlap of the layers occurs when these trajectories coincide with each other (Fig. 11(c)), that may be formulated as the equality of \tilde{H} in the aforementioned states:

$$\tilde{H}(I = I(E_b^{(1)} + \delta_l), \tilde{\psi} = 0) = \tilde{H}(I = I(E_b^{(2)} - \delta_u), \tilde{\psi} = \pi). \quad (55)$$

The asymptotic form of this condition reads as:

$$h \equiv h(\omega_f) = \frac{\sqrt{2}\Phi \ln \left(\frac{4e}{\Phi} \right)}{\pi} \left(\omega_f - \frac{n\pi}{2 \ln \left(\frac{4e}{\Phi} \right)} \right). \quad (56)$$

Both the line (55) and its asymptotic form (56) reasonably agree with the part of the right wing of the spike situated beyond the immediate vicinity to the right from the minimum, namely to the right from the fold at $\omega_f \approx 0.42$. The fold corresponds to the change of the mechanisms of the chaotic layers overlap.

Finally in this section, we will find explicitly the universal shape of the spike in the vicinity of its minimum. With this aim, we linearize the asymptotic lines (22), (52) and (56) in the close vicinity of the spike minimum and present them in terms of the properly scaled amplitude and shift of the frequency from the spike minimum (see also the inset in Fig. 12):

$$\begin{aligned} \tilde{h}(\Delta\tilde{\omega}_f) &= 1 - \sqrt{1 - 4e^{c-2}\Delta\tilde{\omega}_f} \approx 1 - 0.593\Delta\tilde{\omega}_f \\ &\text{for } \Delta\tilde{\omega}_f < 0, \end{aligned}$$

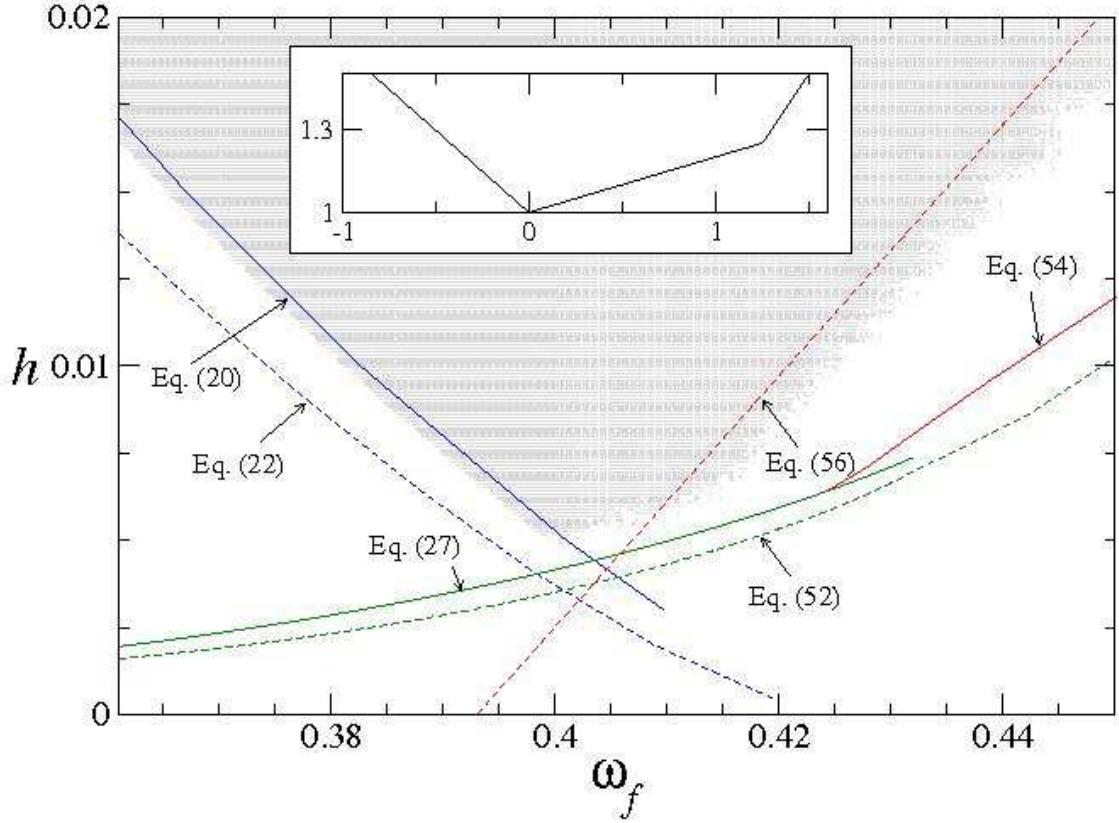


FIG. 12: Comparison of the 1st spike in $h_{gc}(\omega_f)$ derived from numerical simulations (the lower boundary of the shaded area) with the theoretical estimates. The estimates are indicated by the corresponding equation numbers and are drawn by different types of lines, in particular each dashed line represents an explicit asymptote for a solid line of the same color. The inset shows the universal function (57) describing the scaled shape of the spike.

$$\begin{aligned}
 \tilde{h}(\Delta\tilde{\omega}_f) &= 1 + \frac{1 - \sqrt{1 - 4e^{c-2}}}{2} \Delta\tilde{\omega}_f \approx 1 + 0.203\Delta\tilde{\omega}_f \\
 \text{for } 0 < \Delta\tilde{\omega}_f < \Delta\tilde{\omega}_f^{(fold)} &\equiv \frac{2}{1 + \sqrt{1 - 4e^{c-2}}} \approx 1.25, \\
 \tilde{h}(\Delta\tilde{\omega}_f) &= \Delta\tilde{\omega}_f \\
 \text{for } \Delta\tilde{\omega}_f > \Delta\tilde{\omega}_f^{(fold)}, \\
 \tilde{h} &\equiv \frac{h}{h_{s0}}, \quad \Delta\tilde{\omega}_f \equiv \left(\frac{\omega_f}{\omega_{s0}} - 1 \right) \frac{2 \ln\left(\frac{4e}{\Phi}\right)}{c}, \\
 \Phi &\rightarrow 0,
 \end{aligned} \tag{57}$$

where ω_{s0} and h_{s0} are the lowest-order expressions respectively for the frequency and amplitude of the spike minimum given in (40), and c is the constant given in (38) (and in (39)). The fold on the right wing of the spike has the following position:

$$\Delta\tilde{h}^{(fold)} = \Delta\tilde{\omega}_f^{(fold)} = \frac{2}{1 + \sqrt{1 - 4e^{c-2}}} \approx 1.25. \tag{58}$$

We note also that the ratio between all three major slopes of the spike is nicely reproduced by the universal function, as even visually seen from the comparison between the slopes of the lines in the inset and those of the boundary of the shaded area in the main box of Fig. 12.

It follows from (57) that the asymptotic scaled shape is universal i.e. does not depend on either Φ or n . *The derivation of the universal shape of the spike in the vicinity of the minimum is the third major result of the paper.*

V. DISCUSSION OF GENERALIZATIONS AND APPLICATIONS

It is worth mentioning a few possible generalizations:

1. As for an unperturbed system, our major result i.e. the presence of spikes in $h_{gc}(\omega_f)$ can be generalized for an *arbitrary Hamiltonian* system with two separatrices. The asymptotic theory can be generalized accordingly.

2. The absence of pronounced spikes at the *even* harmonics $2j\omega_m$ is explained by the symmetry of the potential (1): the even Fourier harmonics of coordinate q_{2j} are equal to zero. For the time-periodic perturbation of the dipole type, like in Eq. (2), there are no resonances of even order due to this symmetry [1, 2, 3, 4]. If either the potential is *non-symmetric* or the additive perturbation of the Hamiltonian is not an *odd* function of coordinate q , then even-order resonances do exist, resulting in the presence of the spikes in $h_{gc}(\omega_f)$ at $\omega_f \approx 2j\omega_m$.

3. If the time-periodic perturbation is *multiplicative* rather than additive, the resonances become *parametric* (cf. [20]). Parametric resonance is more complicated and much less studied than nonlinear resonance. Nevertheless, the major mechanism for the onset of global chaos remains the same, namely the combination of the reconnection between resonances of the same order and of their overlap in energy with the chaotic layers associated with the barriers. At the same time, the frequencies of the major spikes in $h_{gc}(\omega_f)$ may change (though still being related to ω_m). We consider below the example when the periodically driven parameter is Φ in $U(q)$ (1) [38]. The Hamiltonian reads as

$$\begin{aligned} H &= p^2/2 + (\Phi - \sin(q))^2/2, \\ \Phi &= \Phi_0 + h \cos(\omega_f t), \quad \Phi_0 = \text{const} < 1. \end{aligned} \quad (59)$$

The term $(\Phi - \sin(q))^2/2$ in H (59) may be rewritten as $(\Phi_0 - \sin(q))^2/2 + (\Phi_0 - \sin(q))h \cos(\omega_f t) + h^2 \cos^2(\omega_f t)/2$. The last term in the latter expression does not depend on the dynamical variables and therefore does not affect the equations of motion. Thus, we end up with the additive perturbation $(\Phi_0 - \sin(q))h \cos(\omega_f t)$. In the asymptotic limit $\Phi_0 \rightarrow 0$, the n th-order Fourier component of the function $(\Phi_0 - \sin(q))$ can be shown to differ from zero only for the orders $n = 2, 6, 10, \dots$. Therefore one may expect for major spikes in $h_{gc}(\omega_f)$ to be at the frequencies twice larger than those for the dipole perturbation (2):

$$\omega_{sp}^{(j)} \approx 2\omega_s^{(j)} \approx 2(2j - 1)\omega_m, \quad j = 1, 2, 3, \dots, \quad (60)$$

that well agrees with results of simulations (Fig. 13).

Moreover, the asymptotic theory for the dipole perturbation may be immediately generalized for the present case: it is necessary only to replace the Fourier component of coordinate q by the Fourier component of the function $(\Phi_0 - \sin(q))$:

$$\begin{aligned} (\Phi_0 - \sin(q))_n &= \begin{cases} \frac{4}{\pi n} & \text{at } n=2(2l-1), \\ 0 & \text{at } n \neq 2(2l-1), \end{cases} \\ l &= 1, 2, 3, \dots, \\ \Phi_0 &\rightarrow 0 \end{aligned} \quad (61)$$

(cf. Eq. (12) for q_n). As a result, we obtain:

$$\begin{aligned} \omega_{sp0} &\equiv \omega_{sp0}^{\left(\frac{n+2}{4}\right)} = n \frac{\pi}{2 \ln \left(\frac{4e}{\Phi_0}\right)}, \\ h_{sp0} &\equiv h_{sp0}^{\left(\frac{n+2}{4}\right)} = n \frac{c\pi}{8} \frac{\Phi_0}{\ln \left(\frac{4e}{\Phi_0}\right)}, \\ n &= 2, 6, 10, \dots, \\ \Phi_0 &\rightarrow 0, \end{aligned} \quad (62)$$

where c is given in Eqs. (38) and (39).

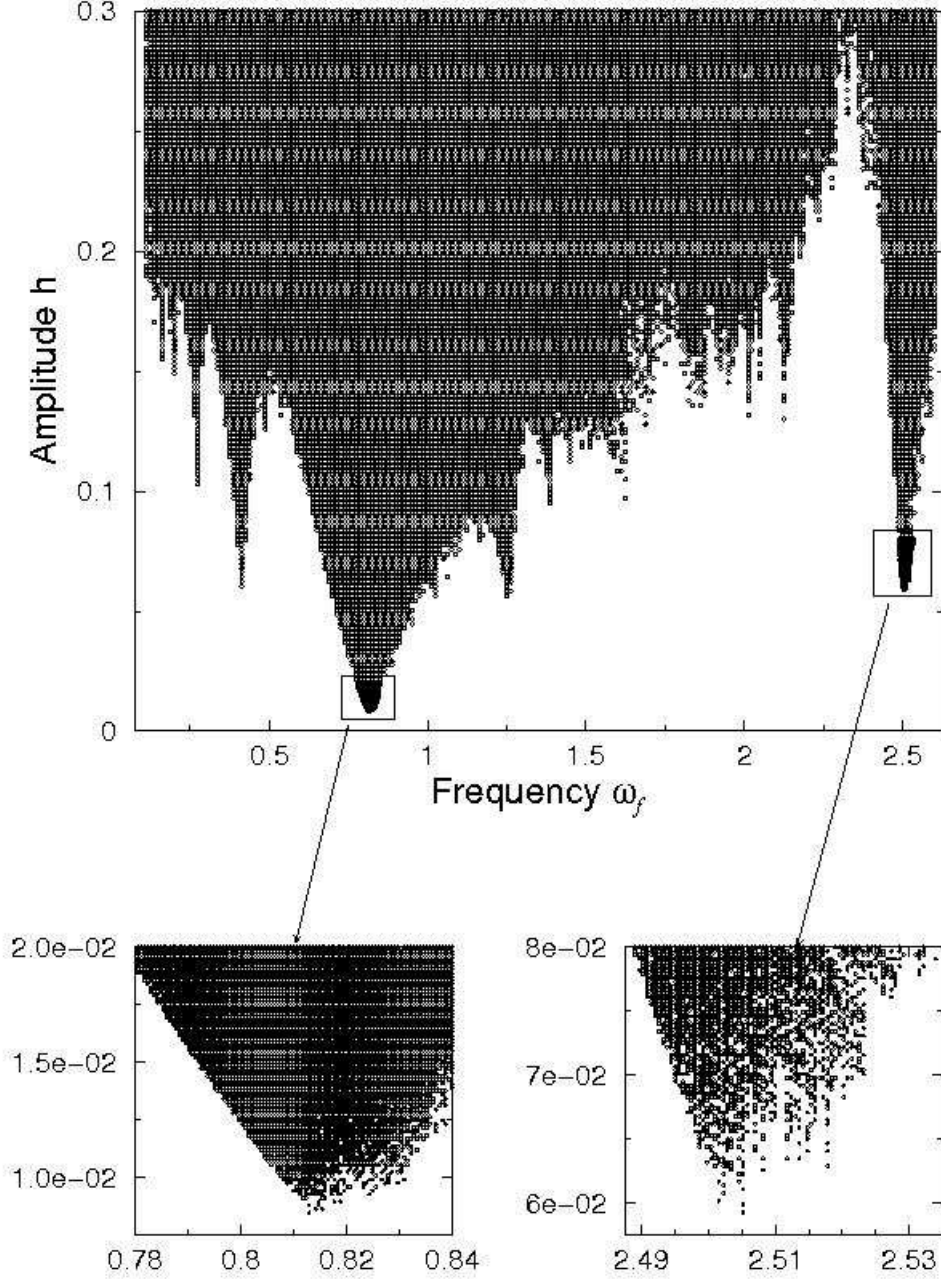


FIG. 13: The diagram similar to that one in Fig.6 but for the multiplicative perturbation i.e. for the system (59) (with $\Phi_0 = 0.2$).

For $\Phi_0 = 0.2$, Eq. (62) gives for the 1st spike the values differing from the simulation data by about 3% for the frequency and by about 10% for the amplitude.

4. Yet more broad generalization relates to *multi-dimensional* Hamiltonian systems with two or more saddles with different energies. Moreover, the perturbation may not necessarily be time-periodic then. The detailed analysis will be done elsewhere.

Finally, we note some far analogy between the facilitation of the global chaos onset described in our work and the so called stochastic percolation in 2D Hamiltonian systems described in the work [39] : the merging of internal and external chaotic zones is also relevant there, like in our case. However, both the models and the underlying mechanisms are very different. Namely, the problem studied in [39] is not of the zero-dispersion type; rather the

two-dimensionality is inherently important.

Let us turn now to examples of possible applications.

A. Electron gas in a magnetic superlattice, spinning pendulum, cold atoms in an optical lattice

The first application relates to the classical electron gas in a magnetic superlattice [14, 15, 16, 17, 18]. In some cases, electrons may be considered as non-interacting quasi-classical particles moving on a plane perpendicular to the magnetic field spatially periodic in one of the in-plane directions (we denote it as x -direction). Then an electron motion in the x -direction is described by the Hamiltonian (1) in which q and p are the properly scaled electron coordinate x and generalized momentum p_x respectively, while the parameter Φ is proportional to the reciprocal amplitude of the external magnetic field, B^{-1} , and to the generalized momentum p_y in the in-plane direction perpendicular to x (see for details [4, 14]). Note that p_y remains constant during the motion [14].

If an ac electric field is applied in the x -direction, then the model (2)-(1) becomes relevant. The *dc-conductivity* in the x -direction is proportional to the fraction of electrons that can take part in the unbounded motion in the x -direction. This fraction, in turn, significantly grows as the range of energies involved into the unbounded chaotic transport increases [14]. In this context, the major result of our paper may be interpreted in the following way. If electrons move in vacuum [40], then it may be possible to inject a beam of electrons which possess one and the same velocity. In this case, the parameter Φ in the model (1) has some certain value, so that the results obtained in the previous sections are immediately applicable. The spikes in $h_{gc}(\omega_f)$ mean the drastic increase of the dc-conductivity occurring at a very weak amplitude of the ac electric field. The frequency of the ac field should be close to one of the spike frequencies. The effect is especially pronounced at the 1st spike i.e. when $\omega_s^{(1)} \approx \pi/[2 \ln(4e/\Phi)]$.

If the electron motion takes place in a semiconductor [14, 15, 16], then the velocity in the y -direction has a *statistical distribution*. The same concerns the parameter Φ then. This might seem to smear the effect: cf. [14] where the *conventional* scenario of the onset of global chaos was exploited. However, in the case of the “zero-dispersion” scenario suggested in our paper, it typically should not be so. Indeed, a statistical distribution of the velocity typically decreases *exponentially sharply* as the velocity exceeds some characteristic value v_c . For high temperature T , the Boltzmann distribution of energy is relevant and, therefore, $v_c \propto \sqrt{T}$. For low temperatures, the Fermi distribution is relevant and, therefore, $v_c \propto \sqrt{E_F}$ where E_F is the Fermi energy. On the other hand, in the range of small Φ , the function $\ln(1/\Phi)$ does not significantly change even if Φ changes by a few times. Hence, if $\Phi_c \ll 1$ (the notation Φ_c means Φ corresponding to v_c), then the value of the partial spike frequency $\omega_s^{(1)}$ is nearly the same for most of the velocities from the relevant range $v_y \lesssim v_c$. Namely, it is approximately equal to $\omega_c \equiv \pi/[2 \ln(4e/\Phi_c)]$. Similarly, $h_s^{(1)} \sim h_c \approx \omega_c \Phi_c/25$. Thus, if one considers the dc-conductivity as a function of ω_f at a fixed $h \gtrsim h_c$, then it will have a sharp maximum at $\omega_f \approx \omega_c$.

If the parameter Φ is time-dependent (e.g. if the external magnetic field has an ac component or/and there is an ac electric force perpendicular to the x -direction), then the applications may be similar, with the only difference that the values of ω_f and h in the minima of the major spikes differ from those for the additive perturbation (see Fig. 13 and its discussion above).

Results of the present paper may also be of an immediate relevance to the pendulum spinning about its vertical axis [19] provided the friction is small. The periodic driving may be easily introduced mechanically, or electrically if the pendulum is electrically charged, or magnetically if the pendulum includes a ferromagnetic material.

Finally, we mention in this subsection that potentials similar to $U(q)$ (1), i.e. periodic potentials with two different-height barriers per period, may readily be generated for cold atoms by means of optical lattices [41]. The dissipation may be nearly completely suppressed by means of the detuning from the atomic resonance [41]. Then results of our paper are of an immediate relevance to such a system too.

B. Noise-induced escape

One more possible application of our results concerns the noise-induced escape over a potential barrier in the presence of a non-adiabatic periodic driving. For a moderately weak damping, such a driving was shown [42] to decrease the activation barrier due to the resonant pushing the system in the range of resonant energies. If the damping is yet smaller, the decrease of the activation barrier becomes larger but due to a different mechanism: it relates typically to the chaotic layer associated with the separatrix of the unperturbed system [4, 43]. The lower energy boundary of the layer is smaller than the potential barrier energy, so that it is enough for the noise to pull the system just to this boundary (rather than to the very top of the potential barrier) after which the system may escape over the barrier purely dynamically. If the eigenfrequency as a function of energy possesses a local maximum, then

the effect may be yet more pronounced [4, 44]: the decrease of the activation barrier may become comparable with the potential barrier at unusually small amplitudes of the driving provided the driving frequency is close to the extremal eigenfrequency. One of the major mechanisms of the latter effect is closely related to phenomena discussed in the present paper, namely, to the overlap of the chaotic layer related to the separatrix of the unperturbed system with the chaotic layer associated with the reconnected nonlinear resonances of the 1st order. In the case of the escape over *two* barriers with different heights, the effect should become even more pronounced due to the mechanism responsible for the spikes of $h_{gc}(\omega_f)$ studied in the present paper. If the potential is periodic, e.g. like in optical lattices [41], the effect may lead to the drastic acceleration of the spatial diffusion.

C. Stochastic web

Finally, let us discuss how our results may be applied to the stochastic web formation [3, 45, 46, 47]. If a harmonic oscillator is perturbed by a plane wave whose frequency is exactly equal to the oscillator eigenfrequency or its multiple, then the perturbation plays two roles [3, 46]. On the one hand, due to the resonance with the oscillator, it transforms the structure of the phase space of the oscillator yielding an infinite number of cells divided by a unique separatrix. It has a form of a web of an infinite radius. On the other hand, the perturbation “dresses” this separatrix by the exponentially narrow chaotic layer (in a mathematical literature, it is often called “stochastic” layer). Such a web-like layer is called *stochastic web*. It may provide for a chaotic transport of the system for long distances both in coordinate and in energy.

In a more typical case, when either the resonance is inexact or/and the unperturbed oscillator possesses a nonlinearity, the perturbation generates *many* separatrices embedded into each other [3, 47], rather than united into one infinite web-like separatrix. Then a significant chaotic transport in energy may arise only if the magnitude of the perturbation exceeds some critical (typically non-small) value corresponding to the overlap of chaotic layers associated at least with two neighbouring separatrices. And, still, the transport in energy remains limited since the width of the chaotic layer around each separatrix sharply decreases as the energy increases. It can be shown [48] that some types of the additional time-periodic perturbation lead to the low-frequency dipole perturbation of the reduced [49] system, like in the system (2)-(1) of the present paper. It is important in the context of our work that the structure of separatrices in the reduced system possesses the property similar to that of the system considered in the present paper. Indeed, in the region between the separatrices, the reduced system performs regular oscillations, and the frequency of such an oscillation as a function of the generalized energy [49] is equal to zero at each of the separatrices. Thus, it necessarily possesses a local maximum between energies corresponding to any two neighbouring separatrices, like in the case considered in the present paper. If the additional perturbation has an optimal frequency related to one of these local maxima, then the overlap of chaotic layers associated with the neighbouring separatrices is greatly facilitated similar to the case considered in the present paper. Moreover, a local maximum of the eigenfrequency changes from pair to pair of separatrices *weakly*, so that even a small excess of the auxiliary perturbation magnitude over the critical value may provide for the simultaneous overlap between *many* chaotic layers. Therefore the distance of the chaotic transport in energy would be greatly increased.

Thus, we conclude that, if the resonance between the oscillator and the perturbation is inexact and/or the oscillator possesses a nonlinearity, then one may greatly facilitate the formation of the stochastic web and make the chaotic transport much more pronounced if one induces an, even rather weak, auxiliary perturbation of the optimal frequency. The same conclusion is valid for so called homogeneous (sometimes called periodic) stochastic webs [3, 45] and many other web-like stochastic structures [3].

It is worth noting that, apart from classical systems, stochastic webs may arise in quantum systems too. It was recently demonstrated, both theoretically [50] and experimentally [51], that the stochastic web may play a crucial role in quantum electron transport in semiconductor superlattices subjected to stationary electric and magnetic fields. Due to the spatial periodicity and a small size of the period, the system possesses electron minibands. It turns out that the description of the electron transport in the lowest miniband may be approximated by the model of the classical harmonic oscillator driven by the plane wave. The role of the harmonic oscillator is played by the cyclotron motion while the wave arises due to the interplay between the cyclotron motion and Bloch oscillations (note that the latter oscillations have an inherently quantum origin). If the cyclotron and Bloch frequencies are commensurate, then the phase space of such a system is threaded by the stochastic web. This gives rise to the delocalization of electron orbits, that leads in turn to the strong increase of the conductivity [50, 51]. However, this effect occurs only when the ratio between the electric and magnetic fields lies in the *exponentially narrow* regions around the values providing for an integer ratio between the Bloch and cyclotron frequencies. Results of our present work suggest the method how to significantly increase the width of the relevant regions. Indeed, if the cyclotron and Bloch frequencies are not exactly commensurate, then the stochastic web does not arise: rather a set of embedded separatrices arises provided the effective wave amplitude is sufficiently large. As discussed in the previous paragraph, even a rather weak

time-periodic driving [52] of the optimal frequency may significantly increase the area of the phase space involved in the chaotic transport. This promises to provide for an effective control of the electron transport in such a system and may be used for developing electronic devices that exploit the intrinsic sensitivity of chaos (cf. [51]). The similar effect may be used also for controlling transmission through other periodic structures, e.g. ultra-cold atoms in optical lattices [53, 54, 55] and photonic crystals [56].

VI. CONCLUSIONS

We have considered in this paper an ac driven spatially periodic potential system with two different-height barriers within the period of the potential. This system represents a characteristic example of a Hamiltonian system possessing two or more separatrices which is subjected to a time-periodic perturbation. A frequency ω of oscillation of the unperturbed motion necessarily possesses a *local maximum* ω_m as a function of energy E in the range between the separatrices. It is smaller than the frequency ω_0 of eigenoscillation in the stable state of the Hamiltonian system by the factor

$$R \sim \ln \left(\frac{1}{\Phi} \right) \gg 1, \quad \Phi \equiv \frac{\Delta U}{U} \ll 1, \quad (63)$$

where ΔU is the difference of energies at the separatrices while U is the difference of energy at the upper separatrix and the energy of the stable state.

The function $\omega(E)$ is close to ω_m in the major part of the energy range between separatrices. Moreover, $\omega(E)$ approaches the *rectangular* form in the asymptotic limit $\Phi \rightarrow 0$. It is this property that provides for the characteristic features of the onset of the global chaos in between separatrices. The major of them is the *drastic facilitation* of the global chaos onset when the perturbation frequency approaches ω_m and/or its multiples: the perturbation amplitude h_{gc} required for the global chaos possesses, as a function of the perturbation frequency ω_f , deep spikes in the vicinity of ω_m and/or its multiples. The mechanism is the following. Due to the rectangular form of $\omega(E)$, two nonlinear resonances of the n th order, that arise if ω_f is slightly smaller than $n\omega_m$, are very wide in energy, even at a rather small h . Thus, even at a rather small h , these resonances may reconnect in the phase space both with each other and with the chaotic layers associated with the separatrices.

The major achievements of the paper are as follows.

1. Combining the separatrix map approach and the resonance analysis, we have developed the self-contained quantitative theory for *boundaries of the chaotic layers in the phase space*. They drastically differ in many respects from those in the conventional single-separatrix case. In particular, unlike the conventional case, the *separatrix split* determines in our case just the *minimal* deviation of the layer boundary from the separatrix while the maximal deviation may be much larger.
2. On the base of the aforementioned theory of the chaotic layers, we have developed the *self-consistent* asymptotic theory describing the *spikes* in the vicinity of the minima. In particular, the *explicit* asymptotic expressions for the very minima are given in Eq. (40). The minimal amplitude h_{gc} is smaller than typical h_{gc} for ω_f beyond the close vicinity of ω_m by the factor $\sim 10R$ where R is given by Eq. (63). The shape of the spike is *universal* and is given by the function (57).

The theory has been verified in computer simulations.

We have also discussed various *generalizations* and *applications*, in particular:

- drastic increase of the *dc-conductivity* of the 2D electron gas in a 1D magnetic superlattice;
- significant decrease of the *activation barrier* for a noise-induced escape over double/multi-barrier structures, that may lead to the drastic acceleration of the *spatial diffusion* in periodic structures;
- strong facilitation of the *stochastic web* formation.

VII. ACKNOWLEDGEMENTS

The work was partly supported by INTAS Grants 97-574 and 00-00867 and by the ICTP Program for Short-Term Visits. We are grateful to Prof. Dominique Escande for discussions. SMS acknowledges the hospitality of Pisa University where a part of this work was done by him.

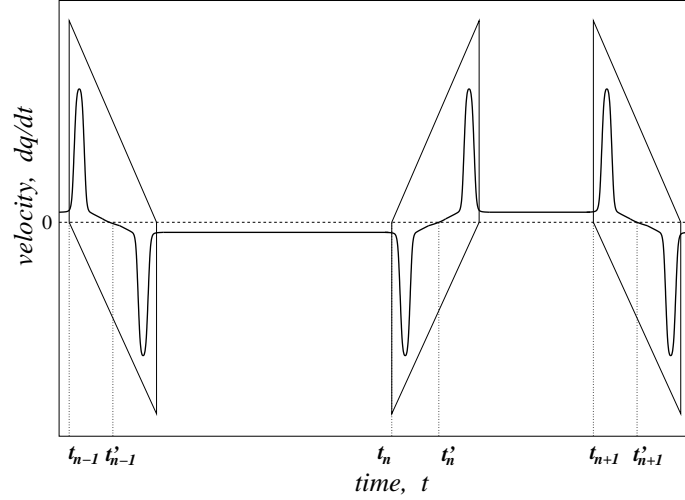


FIG. 14: Schematically shown example of a time dependence of the velocity of the perturbed system (thick solid line) in the case when the energy of motion varies in a close vicinity of the lower potential barrier level. The dashed line marks the zero velocity level. Pulses of the velocity are schematically delineated by the parallelograms (drawn by a thin solid line). Two sequences of time instants $(\dots, t_{n-1}, t_n, t_{n+1}, \dots)$ and $(\dots, t'_{n-1}, t'_n, t'_{n+1}, \dots)$ correspond to beginnings and centres of the pulses respectively.

APPENDIX A: SEPARATRIX MAP

In this Appendix, we describe by means of the separatrix map the chaotic layers of the system (2) associated with the separatrices of the unperturbed system (1). To derive the map, we follow the method described in [3], but some properties of the map for our system in the relevant range of parameters essentially differ from those in the conventional case of a single separatrix [1, 2, 3, 29].

Consider first the *lower* chaotic layer. A typical function $\dot{q}(t)$ for the trajectory close to the inner separatrix (just this separatrix corresponds to the lower potential barrier) is shown in Fig. 14. One can resolve pulses in $\dot{q}(t)$, each of them consisting of two approximately antisymmetric spikes [57]. Pulses are separated by intervals when $|\dot{q}|$ is relatively small. Typically, a duration of a given interval differs from that of the previous interval. Let us introduce the pair of variables E and φ :

$$E \equiv H_0, \quad \varphi \equiv \omega_f t + \varphi_0. \quad (\text{A1})$$

Here φ_0 may be chosen arbitrarily. The energy E changes only during the pulses of $\dot{q}(t)$ and remains nearly unchanged during the intervals between the pulses, when $|\dot{q}(t)|$ is small [3]. We assign numbers n to the pulses and introduce the sequences of (E_n, φ_n) corresponding to initial instants of pulses t_n . In such a way, we obtain the following map (cf. [3]):

$$\begin{aligned} E_{n+1} &= E_n + \Delta E_n, \\ \varphi_{n+1} &= \varphi_n + \frac{\omega_f \pi (3 - \text{sign}(E_{n+1} - E_b^{(1)}))}{2\omega(E_{n+1})}, \\ \Delta E_n &\equiv h \int_{n\text{th pulse}} dt \dot{q}(t) \cos(\omega_f t), \end{aligned} \quad (\text{A2})$$

where $\int_{n\text{th pulse}}$ means the integration over the n th pulse.

Before calculating ΔE_n in a more explicit form, we make two following remarks.

1. Let us denote as t'_n the instant within the n th pulse when \dot{q} turns into zero (Fig. 14). The function $\dot{q}(t - t'_n)$ is an odd function within an n th pulse and it is convenient to transform the cosine in the integrand in ΔE_n (A2) in the following way:

$$\cos(\omega_f t) = \cos(\omega_f(t - t'_n) + \omega_f t'_n) =$$

$$\cos(\omega_f(t - t'_n)) \cos(\omega_f t'_n) - \sin(\omega_f(t - t'_n)) \sin(\omega_f t'_n),$$

and to put $\varphi_0 = \omega_f(t'_n - t_n)$ so that $\varphi_n \equiv \omega_f t'_n$.

2. Each pulse of \dot{q} contains one positive and one negative spike. The first spike can be either positive or negative (cf. Fig.14). If E changes during a given n th pulse such that, its value in the end of the pulse is *smaller* than $E_b^{(1)}$, then the first spikes of the n th and $(n + 1)$ st pulses have the *same* signs. On the contrary, if E in the end of the n th pulse is *larger* than $E_b^{(1)}$, then the first spikes of the n th and $(n + 1)$ st pulses have the *opposite* signs (cf. Fig. 14, which corresponds to the case when the energy remains above $E_b^{(1)}$ during the whole interval presented in the figure). This obviously affects the sign of ΔE_n , and it may be explicitly accounted in the map if to introduce a new discrete variable $\sigma_n = \pm 1$ which is identical to the sign of \dot{q} in the beginning of a given n th pulse,

$$\sigma_n \equiv \text{sign}(\dot{q}(t_n)) , \quad (\text{A3})$$

and changes from pulse to pulse as

$$\sigma_{n+1} = -\sigma_n \text{sign}(E_{n+1} - E_b^{(1)}) . \quad (\text{A4})$$

With the account of the above remarks, we can rewrite the map (A2) as follows (cf. [3]):

$$\begin{aligned} E_{n+1} &= E_n + \sigma_n h \epsilon^{(low)} \sin(\varphi_n), \\ \varphi_{n+1} &= \varphi_n + \frac{\omega_f \pi (3 - \text{sign}(E_{n+1} - E_b^{(1)}))}{2\omega(E_{n+1})}, \\ \sigma_{n+1} &= -\sigma_n \text{sign}(E_{n+1} - E_b^{(1)}), \\ \epsilon^{(low)} &\equiv \epsilon^{(low)}(\omega_f) = \\ &= -\sigma_n \int_{n\text{th pulse}} dt \dot{q}(t - t'_n) \sin(\omega_f(t - t'_n)) \\ &\approx -2\sigma_n \int_{t'_n}^{t_{n+1}} dt \dot{q}(t - t'_n) \sin(\omega_f(t - t'_n)). \end{aligned} \quad (\text{A5})$$

The variable $\epsilon^{(low)}$ introduced in (A5) will be convenient for the further calculations since it does not depend on n in the lowest-order approximation, i.e. both its absolute value and its sign are identical for all pulses. The quantity of the type of $\delta_l \equiv h|\epsilon^{(low)}|$ is sometimes called the *separatrix split* [29] as it determines in the conventional (single-separatrix) case the order of magnitude of a maximal deviation of energy of the chaotic trajectory from the separatrix level. Though we shall also use this term, we emphasize that the maximal deviation in our case may be much larger (see below).

The dynamical chaos appears in the separatrix map (A5) due to the divergence of $|d\omega/dE|$ as E approaches $E_b^{(1)}$. Various heuristic criteria were suggested for the estimate of the width of the chaotic layer, i.e. of the boundaries for the region of $(E - E_b^{(1)})$ inside which the motion is mostly chaotic [2, 3]. One of the criteria [3] is the “stretching” of angle: it suggests that the quantity $|\partial\varphi_{n+1}/\partial\varphi_n - 1|$ should be of the order of 1. Two others [2] relate to the stationary points of the separatrix map. One of the criteria suggests that chaos arises when all stationary points become unstable. Another criterion (more soft) says that the boundary of chaos is related to the onset of global chaos in the maps obtained after the linearization of the separatrix map near its stable stationary points. All these criteria give qualitatively similar results. For the relevant to our problem case of low frequencies, which are much smaller than the reciprocal width of the spikes of $\dot{q}(t)$, the criteria [2, 3] give:

$$|E - E_b^{(1)}| \sim \frac{\omega_f}{\omega_0} h |\epsilon^{(low)}| , \quad \omega_f \ll \omega_0 \approx 1, \quad (\text{A6})$$

where ω_0 is the eigenfrequency in the bottom of the potential well.

However, for the case of small ω_f , the criteria [2, 3] turn out insufficient, so that the estimate (A6) is much lower than the correct one. Indeed, the width of the chaotic layer cannot be less than $h|\epsilon^{(low)}|$: within the range of energies $]E - h|\epsilon^{(low)}|, E + h|\epsilon^{(low)}|[$, even a single iteration of the separatrix map may result in the switch from the range

above the barrier to the range below the barrier or vice versa, and given that the variation of $(\omega(E))^{-1}$ in this range is *infinite*, the interval of time (or equivalently the number of iterations) between successive switches as well as the corresponding changes of angle φ and of energy E may vary from switch to switch random-like.

In the adiabatic limit $\omega_f \rightarrow 0$, the excess of the upper boundary $E_{cl}^{(1)}$ of the lower layer over the lower barrier $E_b^{(1)}$ can be shown [58] (cf. also [59]) to be equal to $2\pi h$. However, ω_f relevant to the spike of $h_{gc}(\omega_f)$ cannot be considered as the adiabatic one, despite its smallness, because it is close to ω_m or to its multiple while the eigenfrequency as a function of energy $E_{cl}^{(1)}$ on the upper outer boundary of the chaotic layer is also close to ω_m at any point of the boundary:

$$\begin{aligned}\omega_f &\approx (2j-1)\omega_m \approx (2j-1)\omega(E_{cl}^{(1)}), \\ j &= 1, 2, 3, \dots\end{aligned}\tag{A7}$$

(the result will confirm this). The validity of (A7) will be essential for the description of the boundary of the layer. Remarkably, this description is quantitative, unlike the conventional single-separatrix case, where the layer width may be estimated in the non-adiabatic case only by the order of magnitude [2, 3].

Let us first find $\epsilon^{(low)}$ in the explicit form. Given that energy is close to $E_b^{(1)}$, the velocity $\dot{q}(t-t'_n)$ in $\epsilon^{(low)}$ (A5) may be replaced by the corresponding velocity along the separatrix associated with the lower barrier, $\dot{q}_s^{(low)}(t-t'_n)$, while the upper limit in the integral may be replaced by the infinity (cf. [3]). Besides, in the asymptotic limit $\Phi \rightarrow 0$, the interval between spikes within the pulse becomes infinitely long [57] and, therefore, only short ($\sim \omega_0^{-1}$) intervals corresponding to the spikes contribute into the integral in $\epsilon^{(low)}$ (A5). In the scale ω_f^{-1} , they may be considered just as two “instants”:

$$t_{sp}^{(1,2)} - t'_n \approx \pm \frac{\pi}{4\omega_m}, \quad \Phi \rightarrow 0.\tag{A8}$$

Therefore, one may substitute the argument of the sinus in the integrand in the definition of $\epsilon^{(low)}$ (A5) by the corresponding constants for the positive and negative spikes respectively, so that

$$\begin{aligned}\epsilon^{(low)} &\approx 2 \sin\left(\frac{\pi\omega_f}{4\omega_m}\right) \int_{\text{positive spike}} dt \dot{q}_s^{(low)}(t-t'_n) \\ &\approx 2\pi \sin\left(\frac{\pi\omega_f}{4\omega_m}\right), \\ \Phi &\rightarrow 0.\end{aligned}\tag{A9}$$

In the derivation of the first equality in (A9), we have also taken into account that the function $\dot{q}_s^{(low)}(t-t'_n)$ is an odd function of its argument. In the derivation of the second equality in (A9), we have taken into account that the right turning point of the relevant separatrix is the top of the lower barrier and the distance between this point and the left turning point of the separatrix approaches π in the limit $\Phi \rightarrow 0$.

For the frequencies relevant to the minima of the spikes of $h_{gc}(\omega_f)$, i.e. for $\omega_f = \omega_s^{(j)} \approx (2j-1)\omega_m$, we obtain:

$$\begin{aligned}\epsilon^{(low)}(\omega_s^{(j)}) &\approx 2\pi \sin\left((2j-1)\frac{\pi}{4}\right) = \sqrt{2}\pi(-1)^{\lfloor \frac{2j-1}{4} \rfloor}, \\ j &= 1, 2, 3, \dots, \quad \Phi \rightarrow 0,\end{aligned}\tag{A10}$$

where the square brackets [...] mean an integer part.

If Φ is just moderately small, then it is better to use the more accurate formula following from the first equality in (A9):

$$\epsilon^{(low)}(\omega_f) = 2 \int_0^\infty dt \dot{q}_s^{(low)}(t) \sin(\omega_f t),\tag{A11}$$

where the instant $t = 0$ corresponds to the turning point of the separatrix to the left from the lower barrier, i.e. $\dot{q}_s^{(low)}(t = 0) = 0$ while $\dot{q}_s^{(low)} > 0$ for all $t > 0$. The dependence $|\epsilon^{(low)}(\omega_f)|$ by Eq. (A11) is shown for $\Phi = 0.2$ in Fig. 15(a). For small frequencies the asymptotic formula (A9) well fits the numerical formula (A11).

Consider now the *dynamics* of the map (A5). For the sake of brevity and clarity, we shall consider the case of ω_f relevant to the 1st spike only ($j = 1$) while the spikes of a higher orders may be considered analogously.

Let the energy at the step $n = -1$ be infinitesimally close to the barrier level $E_b^{(1)}$. The trajectory passing through a state with such an energy is chaotic [1, 2, 3] since $(\omega(E))^{-1}$ diverges as $E \rightarrow E_b^{(1)}$ and, therefore, the angle φ_{-1} is not correlated with the angle on the previous step φ_{-2} . The quantity σ_{-1} is not correlated with σ_{-2} either. Given that $\sin(\varphi_{-1})$ may possess any value from the interval $[-1, 1]$ and σ_1 may equally possess values 1 or -1, the energy may change on the next step for an arbitrary value from the interval $[-h|\epsilon^{(low)}|, h|\epsilon^{(low)}|]$. Thus, $E_0 - E_b^{(1)}$ may be positive and of the order of $h|\epsilon^{(low)}|$. Then, the approximate equality $\omega(E_0) \approx \omega_m$ holds, provided the value of h is from the relevant range. For such E_0 , the further evolution of the map will approximately follow during a long time the trajectory of the auxiliary system (4) with the initial state ($I = I(E_0), \varphi = \varphi_0$). Let us show this explicitly. With this aim, consider two subsequent iterations of the map (A5): $n \rightarrow n + 1$ and $n + 1 \rightarrow n + 2$ with an arbitrary $n \geq 0$. For the sake of concreteness, let $\sigma_n = \text{sign}(\epsilon^{(low)})$ (so that $\sigma_{n+1} = -\text{sign}(\epsilon^{(low)})$). Then,

$$\begin{aligned} E_{n+1} &= E_n + h|\epsilon^{(low)}| \sin(\varphi_n), \\ \varphi_{n+1} &= \varphi_n + \frac{\omega_f}{\omega(E_{n+1})} \pi, \end{aligned} \quad (\text{A12})$$

$$\begin{aligned} E_{n+2} &= E_{n+1} + h|\epsilon^{(low)}| \sin(\varphi_{n+1} - \pi) \approx \\ &\approx E_n + 2h|\epsilon^{(low)}| \sin(\varphi_n), \\ \varphi_{n+2} &= \varphi_{n+1} + \frac{\omega_f}{\omega(E_{n+2})} \pi \approx \\ &\approx \varphi_n + 2\pi + 2\pi \frac{\omega_f - \omega(E_n)}{\omega(E_n)}. \end{aligned} \quad (\text{A13})$$

The approximate equalities in (A13) are due to the validity of (A7) (with $j = 1$). Allowing for the smallness of the quantity $\varphi_{n+2} - \varphi_n - 2\pi$, the map $n \rightarrow n + 2$ (A13) may be approximated by the differential equations

$$\begin{aligned} \frac{dE_n}{dn} &= h|\epsilon^{(low)}| \sin(\varphi_n), \\ \frac{d\varphi_n}{dn} &= \frac{\pi}{\omega(E_n)} (\omega_f - \omega(E_n)). \end{aligned} \quad (\text{A14})$$

Let us (i) use for $\epsilon^{(low)}$ the asymptotic formula (A10), (ii) take into account that the increase of n for 1 corresponds to the increase of time for the half a period $\pi/\omega(E)$, and (iii) transform from the variables (E, φ) to the variables $(I, \tilde{\psi} \equiv -\varphi)$ (note that $dE/dI = \omega(E)$). The equations (A14) reduce then to the following:

$$\begin{aligned} \frac{dI}{dt} &= -h\sqrt{2}\pi \sin(\tilde{\psi}), \\ \frac{d\tilde{\psi}}{dt} &= \omega - \omega_f. \end{aligned} \quad (\text{A15})$$

Equations (A15) are identical to the equations of motion of the system (4) for $n = 1$ in the lowest-order approximation, i.e. to the equations (14) where q_1 is replaced by its asymptotic value (12) and the last term in the right-hand part of the second equation (being of the next order of smallness in comparison with the term $\omega - \omega_f$) is neglected.

The relevant initial conditions for these equations are:

$$\begin{aligned} I(0) &= I(E = E_b^{(1)} + h\sqrt{2}\pi), \\ \tilde{\psi}(0) &= -\varphi_0. \end{aligned} \quad (\text{A16})$$

The angle φ_0 here may be arbitrary.

More generally (when Φ is moderately small), it is better to use more accurate equations (14) and $I(0)$ as

$$I(0) = I(E = 1/2 - \Phi + \delta_l), \quad \delta_l \equiv h|\epsilon^{(low)}|, \quad (\text{A17})$$

with $\epsilon^{(low)}$ calculated by (A11).

We may now analyse the evolution of the boundary of the layer as h grows. Some of the evolution stages are illustrated by Figs. 10 and 11.

So, consider first such values of h that are large enough for the condition (A7) to be satisfied (the explicit criterion will be given in (A19)) but are smaller than the value determined by Eq. (27) (the relevance of this condition will be explained below). Then, the maximum action I_{max} along the regular trajectory (A15)-(A16) is reached at such instant t when $\tilde{\psi}(t) = \pi$. The quantity I_{max} as a function of $\tilde{\psi}(0)$ takes the largest value for

$$\tilde{\psi}(0) = 0. \quad (\text{A18})$$

For the discussed range of h , the outer boundary of the chaotic layer is formed therefore by the trajectory following the dynamical equations (A15) with the initial condition (A16) for action and (A18) for angle, or, more accurately, by the trajectory (14)-(A17)-(A18): see an example in Fig. 10. We note that the minimal value of action on this boundary coincides with the separatrix split level (A17) (asymptotically approximated by (A16)). The necessary and sufficient condition for the second equality in (A7) to hold true at *any* point of the boundary is its validity for the *minimum* energy at the boundary, i.e. for the separatrix split level. The latter condition may be formulated as

$$\omega_m - \omega(E_b^{(1)} + \delta_l) \ll \omega_m, \quad \delta_l \equiv h|\epsilon^{(low)}|. \quad (\text{A19})$$

The condition (A19) determines the lower limit of the relevant range of h . The asymptotic form of (A19) reads as

$$\frac{\ln\left(\frac{\Phi}{h}\right)}{\ln\left(\frac{1}{\Phi h}\right)} \xrightarrow{\Phi \rightarrow 0} 0. \quad (\text{A20})$$

We emphasize that the asymptotic value of h (40) (relevant to the minimum of $h_{gc}(\omega_f)$) satisfies this condition.

As h grows, the boundary of the layer raises up while the lower part of the resonance separatrix, on the contrary, goes down. They reconnect at some critical value of h , $h_{cr}^{(l)} \equiv h_{cr}^{(l)}(\omega_f)$, determined by the condition (27).

If h grows further, then the separatrix split level (A17) becomes higher than the minimal level on the resonance separatrix. As a result, the trajectory (14) with the initial action (A17) and angle (A18) turns out *encompassed* by the resonance separatrix. Obviously, it does not form the outer boundary of the layer anymore. Rather it forms the boundary of the major island of stability inside the layer, repeated periodically in $\tilde{\psi}$ with a period 2π : cf. analogous stability islands in the upper layer in Fig. 10. The *outer* boundary of the layer is formed in this case by the upper (i.e. above the saddle “*sl*”) part of the resonance separatrix. The relevant initial angle $\tilde{\psi}(0)$ corresponds in this case to the intersection between the resonance separatrix and the separatrix split level. Just this case is relevant to the onset of global chaos in the range of ω_f at the close vicinity to the left from the spike minimum: the reconnection of the lower and upper resonance separatrices mark in this case the overlap of the lower and upper chaotic layers (Fig. 11(a)).

If ω_f is shifted further to the left, then, at sufficiently large h , the separatrix split level (A17) may turn out higher than the lower saddle. In this case, the outer boundary of the layer is formed by the trajectory (14)-(A17) with the initial angle

$$\tilde{\psi}(0) = \pi. \quad (\text{A21})$$

In case if ω_f is shifted sufficiently far to the right from the spike minimum, then the resonances disappear or become irrelevant (cf. Fig. 11(c)). In this case, the boundary of the lower layer is formed by the trajectory (14)-(A17)-(A18): cf. Fig. 11(c).

The case of the upper chaotic layer may be treated analogously [60]. We present below just the results for the case $j = 1$.

Let h be large enough for the condition analogous to (A7) to hold true at any point of the lower boundary of the upper layer but, at the same time, let h be smaller than the value of h determined by the condition (28). Then the lower outer boundary of the upper layer is formed by the trajectory following equations of motion (14) with the initial condition (A21) for the angle and (A22) for the action, as given below:

$$I(0) = I(E = E_b^{(2)} - \delta_u), \quad \delta_u \equiv h|\epsilon^{(up)}|, \quad (\text{A22})$$

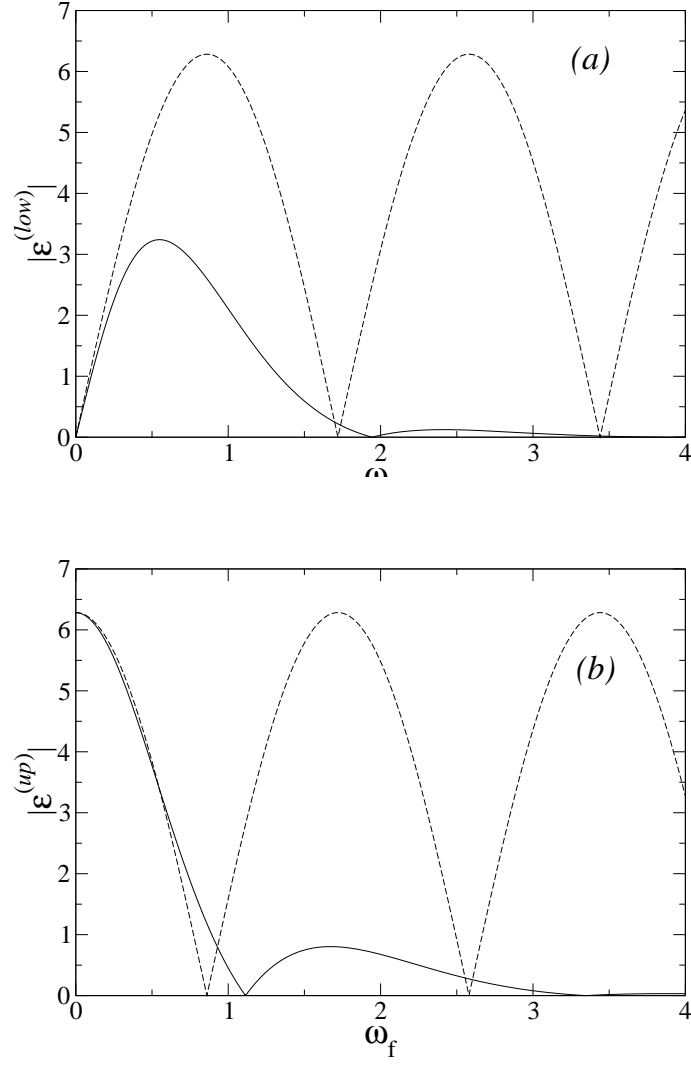


FIG. 15: The theoretical estimates for the normalized separatrix split (for $\Phi = 0.2$) as a function of a perturbation frequency, for the lower and upper layers in (a) and (b) respectively. The solid lines are calculated by Eqs. (A11) and (A25) (for (a) and (b) respectively) while dashed lines represent asymptotic expressions (A9) and (A23) respectively.

where the asymptotic expression for $\epsilon^{(up)}$ at $\Phi \rightarrow 0$ is

$$\epsilon^{(up)} \equiv \epsilon^{(up)}(\omega_f) = 2\pi \cos\left(\frac{\pi\omega_f}{4\omega_m}\right). \quad (\text{A23})$$

For $\omega_f = \omega_s^{(j)} \approx (2j-1)\omega_m$, Eq. (A23) reduces to

$$\begin{aligned} \epsilon^{(up)}(\omega_s^{(j)}) &\approx 2\pi \cos\left((2j-1)\frac{\pi}{4}\right) = \sqrt{2}\pi(-1)^{\lfloor \frac{2j+1}{4} \rfloor}, \\ j &= 1, 2, 3, \dots, \quad \Phi \rightarrow 0, \end{aligned} \quad (\text{A24})$$

where the square brackets [...] mean an integer part.

If Φ is just moderately small, then it is better to use the more accurate formula

$$\epsilon^{(up)}(\omega_f) = 2 \int_0^\infty dt \dot{q}_s^{(up)}(t) \cos(\omega_f t), \quad (\text{A25})$$

where $\dot{q}_s^{(up)}(t)$ is the time dependence of the velocity along the separatrix associated with the upper barrier and the instant $t = 0$ is chosen in such a way that $q_s^{(up)}(t = 0)$ is equal to the coordinate of the lower barrier while $\dot{q}_s^{(up)} > 0$ for $t \in [0, \infty[$. The dependence $|\epsilon^{(up)}(\omega_f)|$ by Eq. (A25) is shown for $\Phi = 0.2$ in Fig. 15(b).

As h grows, the boundary of the layer goes down while the upper part of the upper resonance separatrix, on the contrary, goes up. They reconnect at some critical value of h , $h_{cr}^{(u)} \equiv h_{cr}^{(u)}(\omega_f)$, determined by the condition (28). For larger h , the outer boundary of the upper layer is formed by the lower (i.e. below the saddle “*su*”) part of the upper resonance separatrix (Fig. 10), unless h exceeds the value corresponding to the reconnection of the resonance separatrices (this value of h is determined by the condition (20) or, in the explicit form, (22)). In the latter case (cf. Fig. 11 (b)), the outer boundary of the layer is formed by the part of the resonance separatrix which is situated below the lower saddle “*sl*”. This case is relevant to the close vicinity to the right from the minimum of the spike (Fig. 11(b)).

If ω_f is shifted yet further to the right from the spike minimum, the resonances disappear or become irrelevant (cf. Fig. 11(c)). In this case, the boundary of the upper layer is formed by the trajectory (14)-(A21)-(A22). It is relevant to the part of the spike situated to the right from the fold on the right wing of the spike (Fig. 12): see Fig. 11(c).

-
- [1] B.V. Chirikov, Phys. Rep. **52**, 263 (1979).
[2] A.J. Lichtenberg and M.A. Leibermann, Regular and Stochastic Motion (Springer, New York, 1992).
[3] G.M. Zaslavsky, R.D. Sagdeev, D.A. Usikov and A.A. Chernikov, Weak Chaos and Quasi-Regular Patterns (Cambridge University Press, 1991).
[4] S.M. Soskin, R. Mannella, P.V.E. McClintock, Phys. Rep. **373**, 247 (2003).
[5] J.E. Howard and S.M. Hohns, Phys. Rev. **A 29**, 418 (1984); D. del-Castillo-Negrete, J.M. Greene, P.J. Morrison, Physica **D 61**, 1 (1996); H. R. Dullin, J. D. Meiss, D. Sterling, Nonlinearity **13**, 203 (2000).
[6] J.E. Howard, J. Humpherys, Physica **D 80**, 256 (1995).
[7] More complicated cases are considered e.g. in [4, 6].
[8] Such an overlap is often called the *separatrix reconnection* [4, 5, 6].
[9] D.G. Luchinsky, P.V.E. McClintock, S.M. Soskin, N.D. Stein, A.B. Neiman, Phys. Rev. **E 53**, 4240 (1996).
[10] S.M. Soskin, O.M. Yevtushenko, and R. Mannella, Phys. Rev. Lett. **90**, 174101 (2003).
[11] If there are more than two resonances of the same order, then, for two given neighbouring same-order resonances, other resonances of the *same* order may sometimes play the similar confining role: cf. [6].
[12] S.M. Soskin, O.M. Yevtushenko, and R. Mannella, in *Noise in Complex Systems and Stochastic Dynamics II*, eds. Z. Gingl, J.M. Sancho, L. Schimansky-Geier, J. Kertesz, Proceedings of SPIE Vol. 5471 (SPIE, Bellingham, WA, 2004) p. 355.
[13] Our results may be also generalized for some classes of multi-dimensional time-independent Hamiltonian systems.
[14] O.M. Yevtushenko and K.Richter, Phys. Rev. **B 57**, 14839 (1998); Physica **E 4**, 256 (1999).
[15] H.A. Carmona et al., Phys. Rev. Lett. **74**, 3009 (1995).
[16] P.D. Ye et al., Phys. Rev. Lett. **74**, 3013 (1995).
[17] G.J.O. Schmidt, Phys. Rev. **B 47**, 13007 (1993).
[18] P. Schmelcher and D.L. Shepelyansky, Phys. Rev. **B 49**, 7418 (1994).
[19] A.A. Andronov, A.A. Vitt, S.E. Khaikin, Theory of Oscillators (Pergamon, Oxford, 1966).
[20] L.D. Landau and E.M. Lifshitz, Mechanics (Pergamon, London, 1976).
[21] This value of h is so close to the critical value h_{gc} (the latter is about 0.0048, as seen from Fig. 6) that the blue and green layers nearly touch each other. That is why we did not draw a regular trajectory separating the layers.
[22] We still use different colours for the trajectories starting from $\{I^{(0)}\}$ and $\{O^{(0)}\}$ in order to demonstrate that their mixing occurs very slowly, which indicates that the excess of the given h over the critical value h_{gc} is small [21].
[23] Even harmonics are absent in the eigenoscillation due to the symmetry of the potential.
[24] M. Abramovitz, I. Stegun, Handbook of Mathematical Functions (Dover, New York, 1970).
[25] Note that $E_b^{(1,2)} \approx 1/2 \mp \Phi$ in the first order in Φ .
[26] We neglect here and in Eqs. (10) and (11) the corrections $\sim (\ln(1/\Phi))^{-1}$, since they vanish in the asymptotic limit $\Phi \rightarrow 0$.
[27] The points which correspond just to such stable points of equations (14) are indicated by the crosses in the Poincaré sections shown in Fig. 7.
[28] Note that such neglect is invalid if ω_f/n exceeds ω_m or even is just too close to it. This will be relevant at the consideration of the right wing of the spike: see Sec. IV where we use the exact relations (16) rather than the approximate relation (17).
[29] G.M. Zaslavsky, Physics of Chaos in Hamiltonian systems (Imperial Colledge Press, 1998).
[30] For a given $\omega_f \approx \omega_s^{(j)}$, the numerical error of h_{gc} is rather large since the corresponding simulation involves a very long integration time. We estimate for the relative numerical error of $h_{gc}(\omega_f \approx \omega_s^{(1,2)})$ to be about 10%. Note however that this error practically does not affect the measured values of frequencies $\omega_s^{(j)}$ in the minima of the spikes: the error in the measurement of h_{gc} is systematic while the spikes are very sharp. We estimate for the error of $\omega_s^{(1,2)}$ to be about 1%.
[31] This is because, $\ln[\ln(1/\Phi)]$ is ~ 1 for a *moderately* small value of Φ while a numerical multiplier in the correction

- $\propto 1/\ln(1/\Phi)$ probably has a larger absolute value in comparison with that in the correction $\propto \ln[\ln(1/\Phi)]/\ln(1/\Phi)$. Of course, for sufficiently small values of Φ , the absolute value of the correction $\propto \ln[\ln(1/\Phi)]/\ln(1/\Phi)$ is necessarily larger than that of the correction $\propto 1/\ln(1/\Phi)$.
- [32] Still, such a procedure does not pretend at the completeness since a derivation of some part of the correction of the order of $\ln(1/\Phi)$ requires the use of the second-order averaging method [33], which goes beyond the scope of the present paper. At the same time, even our incomplete procedure gives an excellent agreement with the simulations. This means that the correction originated by the second-order averaging is probably insignificant in comparison with the corrections of other origins.
- [33] N.N. Bogolyubov, Yu. A. Mitropolsky, *Asymptotic Methods in the Theory of Nonlinear Oscillators* (Gordon and Breach, New York, 1961).
- [34] In a general case of an arbitrary potential $U(q)$, when the explicit expression for $q(E, \psi)$ and $\omega(E)$ cannot be obtained, these functions can be calculated numerically.
- [35] We mean that $h_{ge}(\omega_f)$ is smoothed over small fluctuations.
- [36] The function $h_{ge}(\omega_f)$ is slightly lower than the numerically calculated separatrix reconnection line (20) since the chaotic layers associated with the resonances have a small but non-zero width, so that their overlap occurs at slightly smaller values of h than those required for the overlap of separatrices of resonances.
- [37] Given that the relevant values of ω_f may be very close to ω_m , the ignorance of the last term in the left-hand side of the equality in (15) may give rise to a significant inaccuracy if Φ is just moderately small. That is why we take this term into account (see Eqs. (51) and (52)).
- [38] In case of the 2D electron gas in the magnetic superlattice, this may correspond e.g. to the time-periodic electric force applied perpendicular to the direction of the periodicity of the magnetic field [14].
- [39] D.K. Chaikovskiy, G.M. Zaslavsky, *Chaos* **1**, 463 (1991).
- [40] Obviously, such a motion is necessarily three-dimensional. However, if the direction of the magnetic field is perpendicular to the direction of its periodicity, then the motion in the plane perpendicular to the magnetic field is *separated* from the motion along the field. Thus, the in-plane dynamics is two-dimensional while being reduced in the relevant case to the one-dimensional dynamics (2)-(1) (cf. [4, 14]).
- [41] G. Grynberg and C. Milliard-Robilliard, *Phys. Rep.* **355**, 335 (2001); P.H. Jones, M. Goonasekera, and F. Renzoni, *Phys. Rev. Lett* **93**, 073904 (2004); R. Gommers et al. *Phys. Rev. Lett* **94**, 143001 (2005).
- [42] M.I. Dykman, H. Rabitz, V.N. Smelyanskiy, B.E. Vugmeister, *Phys. Rev. Lett.* **79** 1178 (1997).
- [43] S.M. Soskin, R. Mannella, M. Arrayás and A.N. Silchenko, *Phys. Rev.* **E 63**, 051111 (2001).
- [44] S.M. Soskin, R. Mannella, A.N. Silchenko, and M. Arrayás, in *Unsolved Problems of Noise and Fluctuations*, ed. S.M. Bezrukov (American Institute of Physics, Melville, NY, USA, 2003), pp. 421-427.
- [45] A.A. Chernikov, R.Z. Sagdeev, D.A. Usikov, M.Yu. Zakharov, G.M. Zaslavsky, *Nature* **326**, 559 (1987).
- [46] A.A. Chernikov, M.Ya. Natenzon, B.A. Petrovichev, R.Z. Sagdeev, G.M. Zaslavsky, *Phys. Lett.* **A 122**, 39 (1987).
- [47] A.A. Chernikov, M.Ya. Natenzon, B.A. Petrovichev, R.Z. Sagdeev, G.M. Zaslavsky, *Phys. Lett.* **A 129**, 377 (1988).
- [48] S.M. Soskin, unpublished.
- [49] We mean by the *reduced system* the full system averaged over high-frequency oscillations [3, 45, 46, 47] (cf. the system (4) in the present paper). The reduced system is described by the auxiliary Hamiltonian function which may be called the *generalized energy* as it remains constant along any trajectory of the reduced system.
- [50] T.M. Fromhold et al., *Phys. Rev. Lett.* **87**, 046803 (2001).
- [51] T.M. Fromhold et al., *Nature* **428**, 726 (2004).
- [52] It may be induced e.g. by means of a small modulation of the electric field (i.e. an addition of a small ac component to the constant field).
- [53] W.K. Hensinger et al., *Nature* **412**, 52 (2001).
- [54] D.A. Steck, W.H. Oskay, M.G. Raizen, *Science* **293**, 274 (2001).
- [55] R.G. Scott et al., *Phys. Rev. A* **66**, 023407 (2002).
- [56] P.B. Wilkinson and T.M. Fromhold, *Opt. Lett.* **28**, 1034 (2003).
- [57] Spikes correspond to the motion above any of the minima of the potential, first in one and then (after the reflection from one of the upper barriers) in the opposite direction. If Φ is small, the spikes within the pulse are separated by a long interval since the reflection point is situated close to the top of the upper barrier, where the motion is slow.
- [58] S.M. Soskin, O.M. Yevtushenko, and R. Mannella, to be published.
- [59] Y. Elskens and D.F. Escande, *Nonlinearity* **4**, 615 (1991).
- [60] For any ac-driven spatially periodic Hamiltonian system, the *upper* energy boundary of the layer associated with the unbounded separatrix diverges in the adiabatic limit $\omega_f \rightarrow 0$ [61]. However, this divergence is not relevant to the present problem due to the following reasons. The lower chaotic layer relates to the *bounded* separatrix while, for the upper (unbounded) layer, it is the *lower* boundary of the layer that is relevant to the onset of global chaos in between the separatrices. Moreover, even for the upper boundary of the upper layer, the divergence is not yet manifested for the driving parameters (h, ω_f) in the vicinity of the spikes minima (cf. [61]).
- [61] S.M. Soskin, O.M. Yevtushenko, and R. Mannella, *Phys. Rev. Lett.* **95**, 224101 (2005).